Received: 7 February 2018 | Accepted: 18 December 2018
DOI: 10.1002/hyp.13385

WILEY

SPECIAL ISSUE: WATER IN THE CRITICAL ZONE

A low-dimensional model of bedrock weathering and lateral flow coevolution in hillslopes: 2. Controls on weathering and permeability profiles, drainage hydraulics, and solute export pathways

Ciaran J. Harman[1,2] | Cassandra L. Cosans[1]

[1]Department of Environmental Health and Engineering, Johns Hopkins University, Baltimore, Maryland
[2]Department of Earth and Planetary Science, Johns Hopkins University, Baltimore, Maryland

Correspondence
Ciaran J. Harman, Department of Environmental Health and Engineering, Johns Hopkins University, Baltimore, MD.
Email: charman1@jhu.edu

Funding information
National Science Foundation, Grant/Award Number: EAR-1344664, CBET-1360415 and EAR-90072546

Abstract

The advance of a chemical weathering front into the bedrock of a hillslope is often limited by the rate weathering products that can be carried away, maintaining chemical disequilibrium. If the weathering front is within the saturated zone, groundwater flow downslope may affect the rate of transport and weathering—however, weathering also modifies the rock permeability and the subsurface potential gradient that drives lateral groundwater flow. This feedback may help explain why there tends to be neither "runaway weathering" to great depth nor exposed bedrock covering much of the earth and may provide a mechanism for weathering front advance to keep pace with incision of adjacent streams into bedrock. This is the second of a two-part paper exploring the coevolution of bedrock weathering and lateral flow in hillslopes using a simple low-dimensional model based on hydraulic groundwater theory. Here, we show how a simplified kinetic model of 1-D rock weathering can be extended to consider lateral flow in a 2-D hillslope. Exact and approximate analytical solutions for the location and thickness of weathering within the hillslope are obtained for a number of cases. A location for the weathering front can be found such that lateral flow is able to export weathering products at the rate required to keep pace with stream incision at steady state. Three pathways of solute export are identified: "diffusing up," where solutes diffuse up and away from the weathering front into the laterally flowing aquifer; "draining down," where solutes are advected primarily downward into the unweathered bedrock; and "draining along," where solutes travel laterally within the weathering zone. For each pathway, a different subsurface topography and overall relief of unweathered bedrock within the hillslope is needed to remove solutes at steady state. The relief each pathway requires depends on the rate of stream incision raised to a different power, such that at a given incision rate, one pathway requires minimal relief and, therefore, likely determines the steady-state hillslope profile.

KEYWORDS
critical zone, hillslope, lateral flow, weathering

1 | INTRODUCTION

Critical zone science has advanced toward an understanding of the internal architecture of hillslopes, particularly from a geochemical and geophysical perspective (Brantley et al., 2017; St Clair et al., 2015), and a number of hypotheses about drivers of critical zone architecture have recently been articulated (Riebe, Hahm, & Brantley, 2017). Several of these directly address the issue of how chemical weathering in hillslopes is able to "keep pace" with the rate of stream incision into tectonically uplifted bedrock. The lateral movement of water and solutes in the subsurface plays a role in several of these hypotheses (but not all), and there have been general calls for an improved understanding of the role of lateral flow in geochemical weathering processes (Riebe et al., 2017). *Lateral flow* refers to the movement of

water toward the toe of the hillslope rather than strictly vertically. We sometimes speak of lateral flow *partitioning* to refer to the downslope diversion of some portion of vertically percolating water.

Lateral subsurface flow features prominently in the conceptual model presented by Brantley et al. (2017), who argue that where landscapes approach a geomorphic steady state, weathering-induced changes in porosity and permeability, rock fracturing, and surface erosion drive the long-term evolution of water flow paths: ''In effect, we argue that the hill evolves to remove minerals of different solubilities at different surfaces by partitioning water into vertical and horizontal flow paths'' (Brantley et al., 2017). The ''surfaces'' referred to are (a) where weathering is initiated in parent rock at the deepest extent of chemical transformation by meteoric water, (b) an intermediate surface where saprolite transitions to soil, and (c) the land surface. Brantley et al. (2017) argue that the internal partitioning of water between shallow and deep flow paths and overland flow evolves toward a configuration in which all minerals are removed at the same rate: easily dissolved minerals at depth via the slow movement of groundwater, more resistant minerals through dissolution into more rapid lateral interflow perched at the soil–saprolite transition, and most recalcitrant primary and secondary minerals via physical erosion at or near the surface. They liken these surfaces to valves regulating the partitioning of water between two fates: lateral flow that will remove minerals from a surface (through dissolution or erosion) and vertical percolation toward a deeper surface.

Brantley et al. (2017) present detailed arguments about geochemical processes but do not attempt to connect their theory to a mechanistic treatment of flow hydraulics. Other hypotheses have been put forward that emphasize the importance of hillslope hydraulics as both a driver and result of critical zone evolution. Rempe and Dietrich (2014) and Braun, Mercier, Guillocheau, and Robin (2016) make use of hydraulic groundwater theory to build quantitative frameworks predicting the influence of lateral flow on critical zone architecture (for a discussion of Braun et al., 2016, see Harman, Cosans, and Putnam, 2017). Rempe and Dietrich's (2014) model suggests that lateral flow through the unweathered bedrock, driven by its relief above the adjacent stream, could draw reactive water into pores (and even evacuate them when water was not available) at the upper extent of the unweathered rock, initiating weathering. Thus, the rate of stream incision would set the relief of the bedrock that is required for weathering initiation to keep pace with that incision. Rempe and Dietrich (2014) make novel use of well-understood hydraulics and geomorphic principles but do not attempt to connect their theory to quantitative models of geochemical weathering.

Is it possible to develop a simplified but useful treatment of the coupling between weathering and lateral flow that captures both the geochemical and hydraulic controls highlighted by these previous studies? Could the major results of Brantley et al. (2017) and Rempe and Dietrich (2014) fall out of such an analysis as ''special cases'' arising in particular circumstances, thus reconciling them?

Here, we aim to better understand the feedback between lateral flow and weathering and how this feedback influences the architecture of hillslopes. We do so by constructing and analysing a simplified yet physically justified model that captures these feedbacks and can be (approximately) analytically solved in a number of useful cases. This model will enable us to examine how lateral flow might influence the location and properties of weathering fronts within hillslopes, and the internal architecture required to enable lateral flow to export dissolved weathering products at the rate required by stream incision.

This approach can perhaps be criticized along the same lines that all such equilibrium hypotheses in earth science are that they neglect the contingencies of place and the unsteadiness of the climate. Landscapes evolve over long periods with unsteady climatic and tectonic drivers and evolve more rapidly at some periods of time than at others. Steady-state equilibrium is at best a ''convenient fiction'' (Phillips, 2005). Nevertheless, it is a fiction that perhaps we can learn from and use what we learn to make sense of observations from the field.

The paper is structured as follows. Section 2 lays out our simplified model of coupled lateral flow, rock weathering, and the modification of porosity and permeability that it causes. In Section 3, we examine numerical solutions as well as exact and approximate analytical solutions to the model in 1-D vertical sections of an hillslope, under the assumption that advection is large relative to diffusion, paying attention to sensitivity of the results to model parameters relative to a ''base case'' scenario of plagioclase feldspar weathering. These solutions proceed from the simple 1-D infinite column with no lateral flow, to a full solution that includes the modification of permeability by weathering. In Section 4, we then consider diffusion and develop a measure of its importance within the weathering front. We then consider the end-member case that the parent rock is completely impermeable, and so diffusion must play the primary role in weathering and develop an analytical solution applicable to a 1-D vertical section solution for this case, to complement those developed for the advective cases previously.

In Section 5, these pieces are brought together in the context of the whole hillslope morphology. Three end-member ''pathways'' for the export of weathering products are proposed; each of which implies a distinct analytical solution for the longitudinal profile (and overall relief) of the unweathered bedrock surface in a hillslope. The paper concludes by discussing the implications of the results.

2 | SIMPLIFIED MODEL OF FEEDBACKS BETWEEN LATERAL FLOW AND WEATHERING

2.1 | Model assumptions

Building on the hypotheses mentioned above, we are interested in landscapes in geomorphic steady state, such that the rate of weathering is not limited by the rate of chemical reaction or by the availability of meteoric water that can carry solutes away but rather adjusted to the rate of stream incision. This has been described as the ''supply-limited'' case (Riebe, Kirchner, & Finkel, 2004), because the rate of weathering is tied to the rate fresh rock is ''supplied'' by incision. We will further discuss the question of whether our conclusions hold under transient conditions in the discussion and leave full consideration for future work.

There are a number of ways an increase in stream incision might induce a corresponding increase in the pace of chemical weathering. One way is by increasing the rate of surface erosion. This will reduce the proportion of mineral that must be removed by chemical weathering and expose material that is less weathered at the surface where it may contact chemical conditions that can increase the rate of weathering (Riebe et al., 2004). We neglect this case here and choose to focus instead on the case where a mineral is mostly weathered within the hillslope profile. How then can its weathering keep pace with the rate of stream incision?

Lateral flow offers one mechanism that could allow it to do so, as suggested by Brantley et al. (2017). For lateral flow to occur, the pore space must be at or near saturation; otherwise, flow paths are typically exclusively vertical. Weathering that occurs exclusively within the unsaturated zone cannot (in principle) be directly influenced by the effect of stream incision on lateral flow—only regions of the hillslope that are persistently or transiently saturated can.

Unlike the Rempe and Dietrich (2014), the model developed here will not consider the role of surface erosion. Processes operating at the surface and in the unsaturated zone will determine the boundary conditions of the model, but a fully coupled model is left for future work. Many of the arguments that Rempe and Dietrich (2014) make about the coupling between surface weathering and the base of the critical zone also apply to the model presented here.

We also do not consider weathering processes within parts of the hillslope that are freely draining and unsaturated, because weathering processes in freely draining parts of the landscape are likely well approximated by 1-D column models (e.g., Lebedeva, Fletcher, Balashov, & Brantley, 2007). Instead, we focus on those weathering reactions that are primarily limited by the transport of weathering products away from the reaction site, and this transport occurs primarily while the pores are saturated and flow is driven in part by lateral pressure gradients.

As Brantley et al. (2017) and others point out, weathering is not a single chemical reaction. It is not necessarily primarily a dissolution reaction. The reactions do not all occur within a single "weathering zone," below which is pristine parent rock and above which is completely modified saprolite. Because different minerals may weather at different depths, we must stipulate that the model refers to one collection of colocated reactions. Dissolution of plagioclase feldspar will be taken as a prototype "base case." Others may occur below (such as oxidation of biotite) and still more above (such as dissolution of mica). Therefore, when we refer to the "weathering zone," "weathering front," and "weathered" and "unweathered" rock, these should not be taken as absolute terms, rather they are with respect to a particular weathering reaction, perhaps one of several occurring at a range of depths.

2.2 | Further assumptions regarding deep percolation and lateral flow

For lateral flow to occur, there must be a reduction in permeability or a no-flow boundary that prevents the continued (vertical) free drainage of recharge. A weathering front may itself be associated with a small or large change in permeability (perhaps permitting substantial drainage of water below the weathering front, or perhaps only a little) or may occur at a boundary between permeable saprolite and impermeable bedrock. Consequently, we must distinguish between unweathered *permeable* and unweathered *impermeable* rock below the weathering zone. Figure 1 illustrates some of the arrangements we will consider.

Where the weathering front represents a permeability contrast such that the unweathered rock is effectively impermeable, we will consider mechanisms by which reaction products can be removed from the weathering zone through lateral flow within or above the weathering zone. This situation is complicated by the need for there to be appreciable solute transport within a region where permeability is becoming negligible with depth. As we shall see, this is possible through both advection and diffusion of solutes under the right circumstances. Transport of solutes out of the weathering front is simpler if the unweathered material below the weathering front has nonnegligible permeability, so that weathering products can percolate vertically from the base of the weathering front.

In that case, we will assume there exists an additional deeper no-flow boundary within the unweathered material some distance below the weathering front that causes water to be diverted laterally toward the hillslope toe. This boundary will be referred to as *B*. Without such a boundary, the percolating water can freely drain vertically from the base of the weathering zone at a rate limited by the unweathered rock's hydraulic conductivity or by the supply of water from above (in which case, the unweathered rock will be under tension and may become desaturated—this situation is not being considered here, as discussed above). However, deep percolation below the weathering front cannot continue indefinitely, because flow must eventually be diverted laterally toward an outflow location, and so some deeper permeability change or no-flow boundary is a necessary assumption. We will assume that this deep boundary also propagates downward at a rate that keeps pace with the rate of stream incision.

The presence of a no-flow boundary at depth will reduce the percolation from the base of weathering zone by an amount that depends on the thickness and hydraulic gradient of the unweathered rock aquifer toward the outflow location and so provides a connection to channel incision (as suggested by Rempe and Dietrich, 2014, and explored further in Section 5). Here, we will assume this location is the hillslope base, but it may be that the outflow location controlling the drainage hydraulics draws from a larger groundwatershed than surface topography would suggest. In that case, the groundwater "hillslope" considered here may be much larger than a surface hillslope.

There may be a number of physical causes for this deeper boundary *B*, depending on the circumstances. If the weathering front under consideration led to the removal of an abundant but not readily soluble primary mineral (like feldspar), *B* might represents a deeper incipient weathering front where a more soluble mineral is removed or transformed (such as pyrite oxidation), leading to the formation of a permeability contrast at that location. Following the terminology of Brantley et al. (2017), the weathering reaction at *B* would be termed the "profile initiating reaction," whereas the one above would be the "major porosity initiating reaction."

Alternatively, *B* might arise from factors other than weathering. It may be the depth at which topographically induced stress fields open pre-existing fractures (St Clair et al., 2015), or the depth to which

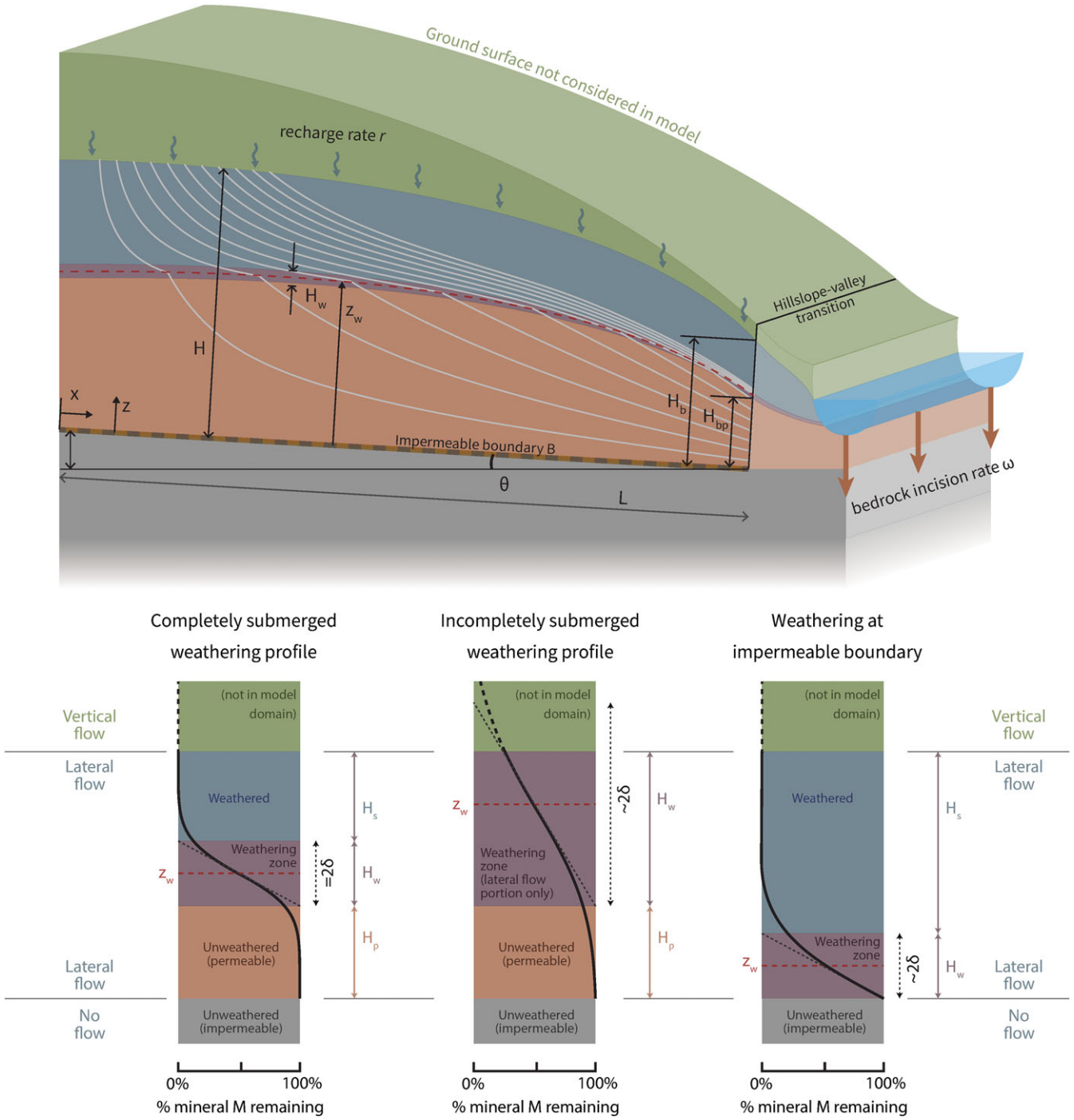

FIGURE 1 Overview of the problem domain and definition of terms. We consider the laterally flowing portion of a hillslope of length L being uniformly recharged from above at rate r with water of constant initial concentration C^H. Rock with initial mineral content M^0 is being weathered, resulting in changes in the porosity ϕ and permeability K. The thickness of the laterally flowing aquifer $H(x)$ above impermeable boundary $B(x)$ (with constant slope θ) can be divided into (up to) three domains: a low-permeability unweathered parent rock $H_p(x)$ (brown coloured zone), a weathering zone $H_w(x)$ (purple), and a zone of more permeable weathered rock $H_s(x)$ (blue). The thickness of these layers varies with location x along the hillslope (measured from the hillslope divide). Parent rock below B is assumed to be impermeable. Boundary conditions are imposed at the downslope boundary of the domain: The full thickness of the laterally flowing zone is H_b; H_{bp} is the thickness of only the weathering and unweathered zones. The entire domain is assumed to be in dynamic equilibrium with an adjacent stream incising into bedrock at rate ω. Elevations are given by a co-ordinate z measured upward from the boundary B. The lower part of the figure shows (left) completely submerged and (right) incompletely submerged profile. We refer to the location where mineral content M is changing the fastest as the weathering "front" z_w. The length scale 2δ is obtained by extrapolating the slope of the weathering front at z_w (fine dotted line). Note that in the incompletely submerged case, the weathering zone H_w is less than 2δ, as H_w only includes weathering in the saturated zone. The model does not consider the behaviour of the system in the freely draining unsaturated part of the profile (green zone, thick dashed line) or the evolution of the ground surface topography

root or frost-cracking damages rock (Anderson, von Blanckenburg, & White, 2007). It may even be the depth of circulation imposed by the regional Tothian groundwater system (Toth, 1963).

In order to make use of the theory developed in the companion paper, Harman and Kim (2018), we will assume that the impermeable surface (whether it is at the base of the weathering zone or at some deeper level) has a relatively small relief. This allows us to assume that the flow system is characterized by a small hillslope number (Hi $\lessapprox$ 1), and so most of the hydraulic gradient driving flow is provided by the mounding of the saturated zone within the hillslope, and not imposed by the geometry of an underlying surface. This is not to say that the ground surface topography is necessarily gentle or that our analysis does not apply in mountainous terrain. The proposed model may apply in steep terrain so long as the slope of the boundary controlling groundwater circulation is not steep.

2.3 | Solute flow and transport

The work presented here builds on the companion paper to this one (Harman & Kim, 2018) in which we showed how hydraulic groundwater theory can be used to construct a model of flow pathways and solute transport through a hillslope at steady state.

In the companion paper, it was demonstrated that in hillslope aquifers with a small hillslope number Hi (Brutsaert, 2005; i.e., those whose impermeable lower boundary has small relief), water age does not increase downslope but instead forms a kind of stack, with oldest water at the impermeable base and youngest water near the recharging surface. As the saturated thickness of laterally flowing water is not constant, the ''layers'' are not of constant absolute thickness but become approximately so when the vertical dimension z is scaled by the saturated thickness $H(x)$ at each location along the slope x (see Figure 1). It was also shown that if other properties (porosity, permeability, and solute source terms) also have this ''scaled lateral symmetry'' (that is they vary exclusively in terms of the scaled co-ordinate $Z = z/H$) then the two-dimensional advection–diffusion–reaction equation collapses into a 1-D vertical equation:

$$\frac{\partial(\phi C)}{\partial t} = -q_z^* \frac{\partial C}{\partial z} + D_m \frac{\partial^2(\phi C)}{\partial z^2} + \phi R, \tag{1}$$

for solute concentration C, where q_z^* is an effective downward flux that varies with z as

$$\frac{\partial q_z^*}{\partial z} = -\frac{q_x}{x}. \tag{2}$$

Note that q_z^* is defined as positive upward, so $-q_z^*$ represents the downward flux rate. The lateral flux rate q_x is approximated using the Dupuit approximation for the hydraulic gradient term ∇h:

$$q_x = -K\frac{dh}{dx} \tag{3}$$

$$= H'(x)\cos\theta - \sin\theta, \tag{4}$$

where $H'(x)$ is the gradient of saturated thickness, θ is the angle the (assumed impermeable) base of the aquifer makes with the horizontal, and K is the hydraulic conductivity. We will assume that permeability is isotropic, even where it is not homogeneous in space (and so K is a scalar, not a tensor). The lateral flow rate q_x may vary with z as K changes, but under the Dupuit assumption, the lateral hydraulic gradient ∇h is invariant in z.

2.4 | Simplified kinetic model of rock weathering

There has been significant progress in understanding and quantifying rock weathering reactions over recent decades (Maher, 2011; Riebe et al., 2017; White & Blum, 1995; Murphy, Oelkers, & Lichtner, 1989). That understanding has matured through numerical models of reactive transport in 1-D, as in a reaction column, where the flux rate of water through the column is constant in space and time. This has led to the development of simplified kinetic models of rock weathering that capture some emergent properties of 1-D weathering profiles.

Here, we will adapt one such simplified model of rock weathering (similar to, e.g., Lebedeva, Fletcher, & Brantly, 2010; Li, Jacobson, & McInerney, 2014) and apply it to the lateral flow model described above. The transformation of primary minerals into dissolved products is given by the rate of primary mineral consumption R_j:

$$\frac{\partial M_j}{\partial t} = -R_j = -k_j M_j \left(1 - S_j\right), \tag{5}$$

where M_j (mol m^{-3}) is the moles of mineral j per control volume of porous media (i.e., solid plus pore volume), S_j is a saturation index that is 1 when the aqueous phase is in equilibrium with the primary mineral, and k_j (year^{-1}) is a reaction rate. The reaction rate is related to the specific surface area of the mineral as

$$k_j = k_j^* F_j A_j, \tag{6}$$

where k_j^* (mol m^{-2} year^{-1}) is the area-specific reaction rate, F_j is the molecular (formula) weight (g mol^{-1}), and A_j is the specific surface area (m^2 g^{-1}), which (following Li et al., 2014; White & Blum, 1995; White & Brantly, 2003) can be estimated by $A_j = 6\beta_j/(\rho_j D_j)$ assuming spherical particles with an effective grain diameter D_j, density ρ_j, and a surface roughness factor β_j. We will assume that these factors are constant (though they likely vary as the rock weathers).

The rate of production R_i of a particular dissolved weathering product with concentration C_i is related to the weathering rate as

$$R_i = \frac{n_{ij} R_j}{\phi}, \tag{7}$$

where n_{ij} is a stoichiometric ratio of moles of product released per mol of primary mineral consumed, and porosity ϕ accounts for the differing volumes used to normalize C_i (the fluid-filled pore volume) and M_j (the total porous media volume).

Finally, we assume that the saturation index S_j is primarily determined by the production of a single aqueous phase, such that we can approximate:

$$S_j \approx \frac{C_i}{C_{ij}^{eq}}, \tag{8}$$

where C_{ij}^{eq} is the equilibrium concentration of i with respect to j at saturation.

2.5 | Effect of weathering on porosity and hydraulic properties

Unfortunately, there is not currently a well-developed parsimonious approach to modelling the effects of weathering on rock hydraulic properties that we are aware of, at least not one grounded in observational and modeling studies of rock weathering. Certainly, the dissolution of minerals can increase porosity, and relations like the Kozeny–Carmen equation (Carmen, 1837; Kozeny, 1927) provide relationships between porosity and permeability, but there are potential complications. Minerals can react nonisovolumetrically (Nettleton, Flach, & Nelson, 1970), and saprolite may volumetrically expand or collapse as it is modified by chemical and physical weathering (Parizek & Girty, 2014), complicating the relationship between porosity and the degree of weathering. The precipitation of secondary minerals can infill pores and reduce porosity (Navarre-sitchler, Steefel, Yang, Tomutsa, & Brantley, 2009). Furthermore, it is necessary to know which pores become infilled. Permeability will be much less reduced by the infilling of less connected or fine pores than large pores or pores with high connectivity. Consequently, it is not clear whether simple relationships like the Kozeny–Carmen relation, or other equations derived for "packed spheres" or such idealizations (Xu & Yu, 2008), can be applied.

Unfortunately, there are not clearly superior options at this point. Therefore, to make progress, we will assume isovolumetric weathering and account for the feedback in a simplistic way by assuming porosity increases linearly as primary minerals are dissolved:

$$\phi = \phi_0 + \phi_m \left(1 - \frac{M}{M^0}\right), \tag{9}$$

where ϕ_0 is the porosity of the parent rock, ϕ_m is the porosity once weathering is complete, and M^0 is the mineral content of parent rock. We crudely account for the effect of infilling by secondary mineral precipitation by setting $\phi_m = M_j^0 F_j \rho_j - \phi_s$, where ϕ_s is the infilled porosity.

In the absence of a better approach, we assume that conductivity K varies with porosity ϕ according to the Kozeny–Carman relationship: $K \sim \phi^3/(1-\phi)^2$. To set a value for the coefficient in this relationship, we will assume the conductivity of the parent rock K_0 is known, and so

$$K = \left(K_0 \Big/ \frac{\phi_0^3}{(1-\phi_0)^2}\right) \frac{\phi^3}{(1-\phi)^2}. \tag{10}$$

The rate conductivity increases with porosity is consequently highly sensitive to the parent rock porosity.

2.6 | Scaled lateral symmetry and boundary conditions

The system of differential equations given by (1), (2), and (5) can be solved if an appropriate set of parameters and initial and boundary conditions are supplied. We must be careful however to ensure that these parameters and conditions do not violate the assumption of scaled lateral symmetry used to derive Equations 1 and 2 in the companion paper. Equation 5 does not break the scaled lateral symmetry if we assume its parameters are spatially constant, and so the variations in M_j arise endogenously due to interactions with C_i and q_z. In addition, we assume that the rate and concentration of recharge are invariant in x, as are the composition and properties of the parent material.

2.7 | Traveling wave formulation

Steady-state solutions to the equations above take the form of a traveling wave, much like those investigated by Ortoleva, Chadam, Merino, and Sen (1987) and Lichtner (1988). Let us assume that the wave is traveling in the $-z$ direction (downward) at rate w and define $z' = z + wt$ as a spatial co-ordinate traveling with that wave. Applying this to the system of equations above, we find that the rate of change of C, M, and q_z with respect to z' can be expressed as

$$\frac{\partial M}{\partial z'} = -\frac{R}{w}, \tag{11}$$

$$\frac{\partial C}{\partial z'} = -\frac{nR}{(-q_z^*) - w\phi}\left(1 - \frac{C\phi_m}{nM^0}\right) + \frac{D_m}{(-q_z^*) - w\phi}\frac{\partial^2 \phi C}{\partial z'^2}, \tag{12}$$

$$\frac{\partial q_z^*}{\partial z'} = -\frac{K|\Delta h|}{x}, \tag{13}$$

where z' and q_z^* are both positive upward and negative downward, and $|\nabla h| \geq 0$. The reaction rate R is given by (5), the porosity ϕ by (9), and the conductivity by (10). Spatial derivatives of ϕ have been simplified in this equation using (9) and (5). The i and j subscripts have been omitted for clarity. From this point on, the prime will be omitted from z, and all equations will be expressed in terms of the moving frame of reference.

2.8 | Numerical solution

The equations above can be solved numerically, though some care is needed to properly account for the boundary conditions. Solutions must be found iteratively if the diffusion term is included. If we neglect the effects of diffusion, the second term in (12) disappears and only first-order spatial derivatives remain, so the equation can be solved as a system of ordinary differential equations. Here, we solved them in Python using the SciPy function scipy.integrate.ode, which provides an interface to the LSODA integrator (Jones, Oliphant, & Peterson, 2001).

We typically choose values of the recharge concentration C^H at the top of the saturated zone $z = H$ and the parent rock composition M^0 at the base $z = 0$. However, these values are specified at opposite ends of the domain (making this a boundary value problem). To proceed, we chose an initial guess for M^H at $z = H$ and integrated in the $-z$ direction to $z = 0$. The value of M^H was then adjusted until the computed value of M at $z = 0$ reached the desired value M^0. This is essentially a "shooting method" (Roberts & Shipman, 1972).

2.9 | Base case parameters

In the remainder of this paper, we will present numerical and analytical solutions to the equations above using (unless otherwise specified) a base case set of parameters representative of plagioclase feldspar

weathering (parameters are listed in Table 1). These parameter values are taken from Li et al. (2014), White and Brantley (2003), and references therein.

3 | INSIGHTS FROM ANALYTICAL SOLUTIONS (ADVECTION ONLY)

Equations 11, (12), and (13) can be solved numerically, but insights can also be gained by investigating exact and approximate analytical solutions that arise under various assumptions. Below, we will develop such several solutions and discuss the insights they generate into controls on the location and thickness of the weathering front in a 1-D vertical "slice" of a hillslope at a given lateral co-ordinate *x*, or where the thickness of the saturated zone $H(x)$ is known. In this section, we will assume that diffusion is not important. The next section will consider the case where it dominates.

We will use the terms *weathering front* and *weathering zone* throughout the remainder of this paper. Weathering front refers to the location of the steepest rate of change of M with depth, which is also (by definition) the inflection point of the curve describing M. The weathering zone should be taken as shorthand for the *submerged* weathering zone. It is the region around the weathering front in which M is changing appreciably with depth *within the saturated zone*. For simplicity of expression in the discussion, the term excludes the region above the saturated zone, as it is outside the domain of the model considered here. The region above may be unsaturated saprolite or soil in which weathering continues to take place, or it may be that the upper extent of saturation coincides with the ground surface, which is being lowered by erosion. Regardless the term 'weathering zone' will only refer to the region within the model domain.

3.1 | 1-D vertical-only flow

To begin, we can consider a case that is already well studied: that of flow in a column without lateral flow. If we assume that the horizontal flux is zero $q_x = 0$, Equation 13 shows that the vertical flux rate q_z must be constant. Assuming variations in ϕ can also be neglected, there is an exact solution to the system of differential equations:

$$C(z) = C^{eq}\left(1 - \left(\frac{w}{k\delta}\left(1 + \tanh\left(\frac{z - z_w}{\delta}\right)\right)\right)\right) \tag{14}$$
$$M(z) = \frac{C^{eq}}{kn\delta}(-q_z^* - \phi w)\left(\left(1 - \tanh\left(\frac{z - z_w}{\delta}\right)\right)\right).$$

This solution can be checked by substituting it into the equations above. Li et al. (2014) obtained an equivalent solution, though their formulation is slightly different. Here z_w [L] and δ [L] are constants of integration.

These functions are sigmoidal curves centred on z_w, in the sense that at z_w, the rate of change of both curves is greatest. We will refer to z_w as the "location" of the weathering front, although the weathering may be substantial at that point. The value of δ controls the steepness of the weathering front, with small δ implying a sharp front and large δ implying a broad, gradual front. The precise relationship of z_w and δ to other parameters will depend on the boundary conditions applied.

3.1.1 | Infinite column

In the simplest case, we could assume that the system is effectively infinitely long, with $C = C^H$ at $z = \infty$, and $M = M^0$ (the parent rock mineral content) at $z = -\infty$. The "location" for the weathering front relative to the origin is arbitrary, as it is not constrained by any point of reference. We can therefore choose to say that at $z = z_w$ the rock

TABLE 1 Base case parameters representative of plagioclase feldspar weathering, along with assumed hillslope, recharge, and landscape incision rates

Parameter		Base-case value	Units	Description
k^*	=	2.5×10^{-6}	mol m^{-2} year^{-1}	Area-specific reaction rate
F	=	265.44	g mol^{-1}	Formula weight
β	=	9	-	Surface roughness factor
ρ	=	2.66×10^{6}	g m^{-3}	Mineral density
D	=	2×10^{-4}	m	Mineral grain diameter
ϕ_0	=	0.15	-	Porosity of parent rock
ϕ_s	=	0.215	-	Final volume of secondary mineral precipitation
n_{ij}, n	=	0.8	-	Stoichiometric ratio
D_m	=	0.0315	m^2 year^{-1}	Molecular diffusion coefficient
C^{eq}	=	9.68×10^{-1}	mol m^{-3}	Equilibrium concentration
M^0	=	3.16×10^{3}	mol m^{-3}	Mineral content of parent rock
C^H	=	0	mol m^{-3}	Concentration of recharge
K_0	=	11	m year^{-1}	Permeability of unweathered rock
r	=	0.3	m year^{-1}	Recharge rate
L	=	250	m	Hillslope length
x	=	25		Location along hillslope from divide
$\lvert\nabla h\rvert$	=	0.03		Total hydraulic head gradient
H_b	=	4	m	Depth of circulation below stream/valley
ω	=	3×10^{-5}	m year^{-1}	Rate of stream/valley incision

is half weathered ($M = M^0/2$). Substituting these into (14) provides a system of equations that can be solved to give:

$$w = (-q_z^*) \times \frac{C^{eq} - C^H}{M^0 n + \phi C^{eq}}, \tag{15}$$

$$\delta = \frac{2w}{k}, \tag{16}$$

where $(-q_z^*)$ is the steady flow rate through the column. Substituting these into (14) gives

$$C(z) = C^{eq} \times \frac{1}{2}\left(1 - \tanh\left(\frac{z - z_w}{\delta}\right)\right), \tag{17}$$

$$M(z) = M^0 \times \frac{1}{2}\left(1 - \tanh\left(\frac{z - z_w}{\delta}\right)\right). \tag{18}$$

The term $\frac{1}{2}(1 - \tanh(\cdot))$ has a sigmoidal form that varies from 1 at $-\infty$ to 0 at ∞. The maximum rate of change is located at $z = z_w$ and is equal to $1/(2\delta)$. About 75% of the change in C and M occurs over a distance of 2δ between $z = -\delta$ and $z = \delta$ (about 96% occurs in a range of 4δ). As the lower panels in Figure 1 suggest, 2δ is the distance that would be required for M to go from 0% weathered to 100% if it were changing (in space) at the maximum rate.

The rate of weathering front propagation w in this case is a well-known expression (Lichtner, 1988) that arises from the balance between the supply of weatherable material to the reaction front as it propagates, $wM^0 n$, and the rate they are carried away by the moving fluid phase, $q_z^* C^{eq}$. The term ϕC^{eq}) added to the denominator accounts for the equilibrated pore fluid that arrives with the supply of weatherable material and can be ignored because it is much smaller than $M^0 n$.

3.1.2 | Finite column

Moving closer to a realistic scenario, we could instead assume that we are interested in a finite "window" of weathered and weatherable material that extends from an upper location (at $z = H$) where the concentration of fluid is known to a location at depth ($z = 0$) where rock is unweathered. The value of M is fixed at $z = 0$, where unweathered rock is entering the window, at $M(0) = M^0$, and C is fixed where flow enters at $C(H) = C^H$. Conversely, the aqueous concentration $C(0) = C^0$ (not necessarily at equilibrium) and primary mineral remaining $M(H) = M^H$ (not necessarily zero) are not known.

Let us further assume this window moves in the direction of flow (i.e., in the negative z direction) at some known fixed rate w. The shape of the weathering front (i.e., the profile of $C(z)$ and $M(z)$) will need to simultaneously conform to the boundary conditions, and weather rock at a sufficient rate that dynamic steady state is achieved at this rate of progression w. This may be feasible for only some combinations of parameters.

Substituting the finite column boundary conditions into (14) yields solutions for z_w and δ, and $C(z)$ and $M(z)$ that are determined by a set of implicit equations. We can first define for convenience the sigmoidal function:

$$S(z) = \frac{1}{2}\left(1 - \tanh\left(\frac{z - z_w}{\delta}\right)\right). \tag{19}$$

Using this, implicit equations determining z_w and δ can be written as

$$-q_z^* = w\eta \times \frac{1 - S(H)}{S(0)}, \tag{20}$$

$$\delta = \frac{2w}{k} \times \frac{C^{eq} - S(H)C^{eq}}{C^{eq} - C^H}, \tag{21}$$

and the solutions for $C(z)$ and $M(z)$ are given by solving

$$\frac{C^{eq} - C(z)}{1 - S(z)} = \frac{C^{eq} - C^H}{1 - S(H)}, \tag{22}$$

$$\frac{M(z)}{S(z)} = \frac{M^0}{S(0)}. \tag{23}$$

Some simplification has been introduced based on the assumption that the mineral is relatively abundant and insoluble, so $M^0 n \gg \phi C^{eq}$. The dimensionless quantity

$$\eta = \frac{M^0 n}{C^{eq} - C^H} \tag{24}$$

represents the volume of water at initial concentration C^H that would be required to fully weather a unit volume of rock with initial content M^0. It varies inversely with solubility of the rock in the inflowing water and can be thought of as the resistance of the rock to dissolution. Recharge arrives with concentration C^H and can dissolve weathering products until it reaches concentration C^{eq}. The amount it must dissolve (per unit of volume rock) in the parent material is $M^0 n$.

The location of z_w in this finite column case turns out to be highly sensitive to the dimensionless ratio $w\eta/(-q_z^*)$ in (20), which represents the balance between the rate that weatherable minerals are moving into the window $0 < z < H$, and the rate dissolved products are removed if the inflowing water is allowed to reach equilibrium. Equation 15 is equivalent to $w\eta/(-q_z^*) = 1$, showing that this balance holds in the infinite case regardless of the values of z_w and δ. Here, this $w\eta/(-q_z^*)$ ratio needs not necessarily be equal to 1 (though it must be close), but z_w and δ must be chosen so that Equation 20 is satisfied. When $w\eta/(-q_z^*)$ is large, z_w is close to H, and considerable residual unweathered mineral M^H remains at the top of the column at $z = H$ and passes out of the solution domain. Conversely, when it is small, z_w is close to 0, and the fluid may not have a chance to reach equilibrium before it leaves. For values of $w\eta/(-q_z^*)$ that are too small or too large, there may be no value of z_w that satisfies the boundary conditions.

This behaviour can be understood intuitively as arising from the limited degrees of freedom available for the solution to satisfy the requirement that the weathering front propagate at rate w. It can only modify the values of the outflow concentration C^0 or the residual mineral content M^H. If the thickness of the weathering front is small compared with H, then z_w can be chosen to modify C^0 or M^H substantially away from their asymptotic values ($C^0 \to C^{eq}$ and $M^H \to 0$), but not both. The thickness of the front is on the order of 2δ, which is (again) approximately $4w/k$ by Equation 21. Thus, if the front is to advance "slowly" ($w > (-q_z^*)/\eta$), z_w must be within a distance $4w/k$ of the top of the column ($z = H$) so that the weathering front is not required to fully weather the rock before it passes out of the domain ($M^H > 0$). If it must advance "quickly" ($w < (-q_z^*)/\eta$), z_w must be within

a distance $4w/k$ of the bottom of the column ($z = 0$) so that the fluid reacting with the fresh rock is far from equilibrium ($C^0 < C^{eq}$).

3.2 | Lateral flow—homogeneous *K*

Let us now consider the case of a homogeneous aquifer but ignore the effect of feedbacks with permeability and porosity (this will be relaxed in subsequent sections). The key difference between this and the column considered above is that in this case, the fluid flux rate is not a constant, but instead varies in z. This makes it possible to look for a value of z_w that provides the "right" flux rate to carry solutes away at the rate required by the supply of fresh rock and satisfies the boundary conditions.

This reasoning is the basis for the approximate analytical solution for a homogeneous aquifer provided in this section. The solution is based on the assumption that the vertical flux rate is relatively constant within the weathering front, but that flux rate is the "right" one.

Let us assume that the aquifer is draining to a stream that is incising at rate ω. To maintain dynamic steady state, the weathering front advance rate must "keep up" with incision rate, so $w = \omega$. The elevation of the impermeable surface at $z = 0$ is also assumed to lower (through an unspecified process) at the rate of stream incision, so that its position relative to the stream is constant.

In order to propagate at rate ω, the weathering front must be at the location within the hillslope where the flux is sufficient to remove weathering products at the rate they are supplied. The effective vertical flux rate in a homogeneous aquifer varies linearly with depth as $-q_z^* = r\frac{z}{H}$ (see companion paper Harman and Kim, 2018). We will therefore assume that the flow rate at the inflection point of the weathering front z_w is

$$-q_z^*(z_w) = r\frac{z_w}{H}, \tag{25}$$

where r is the recharge at the top of the saturated zone. Let us assume this rate is approximately constant across the weathering zone and substitute it into the general solution (14), along with the requirement that $w = \omega$. This yields a solution similar to the previous one, except that now,

$$\frac{z_w}{H} = \frac{\eta\omega}{r} \times \frac{1 - S(H)}{S(0)}, \tag{26}$$

$$\delta = \frac{2\omega}{k} \times \frac{C^{eq} - S(H)C^{eq}}{C^{eq} - C^H}. \tag{27}$$

Figure 2 shows the relationship between z_w/H and H for a number of cases of $\omega\eta/r$ predicted by this analytical approximation. To calculate each curve in the plot, the base case parameters $\omega = 30$ m Ma^{-1} and $r = 0.3$ m year^{-1} have been held fixed, and the weathering resistance term η has been varied between curves. The curves were determined by varying the gradient $|\Delta h|$ to obtain a range of aquifer thicknesses H at $x = 25$ m (varying $|\Delta h|$ means the total flux crossing the modeled profile is held constant, but the flux per vertical unit of distance is varied). Figure 2b,c shows the full profiles of $C(z)$ and $M(z)$ for the case of $H = 10$ m for both the numerical and approximate analytical solutions. The results are very close to one another in most cases. They diverge only for $C(z)$ close to the bottom boundary, where $-q_z^*$

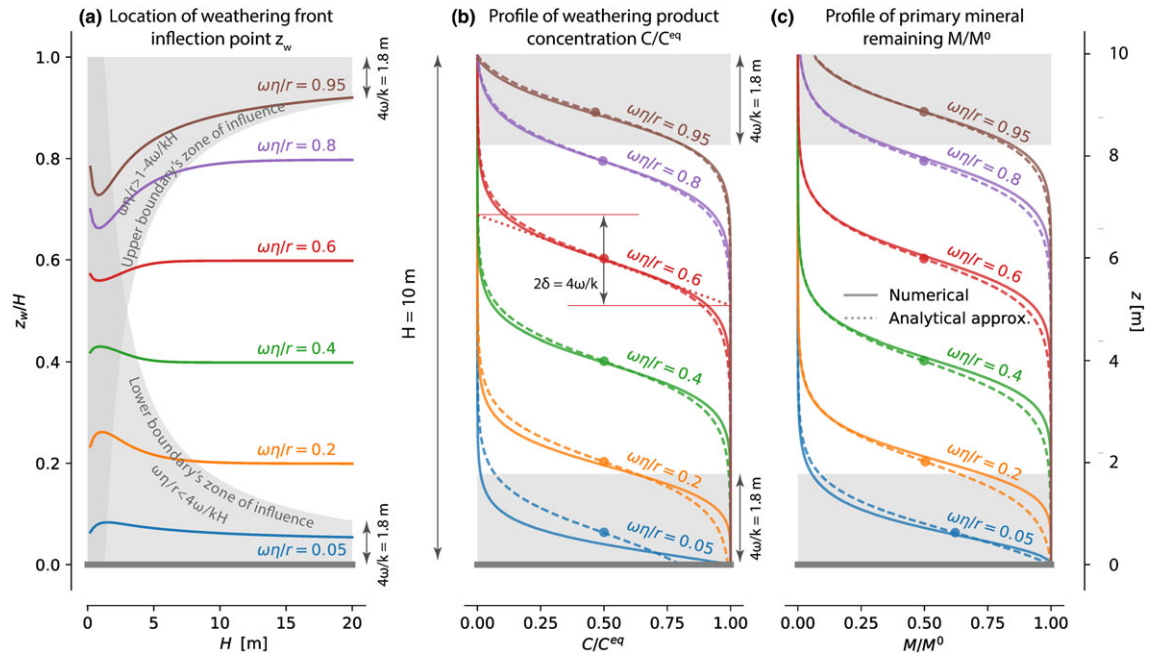

FIGURE 2 Weathering fronts in the absence of feedbacks with porosity and permeability for base case parameters, with diffusion neglected. (a) The location of the steepest part of the weathering front z_w as a proportion of the saturated thickness H is determined primarily by the dimensionless ratio $\omega\eta/r$. There is some sensitivity to the saturated thickness H because the boundary conditions at $z = 0$ and $z = H$ can influence the shape of the front (rather than just its upper and lower limits) if $H\omega\eta/r$ is within a distance $4\omega/k$ of the boundary. For the base case parameters $4\omega/k = 1.8$ m. (b,c) The analytical approximation given by (26) and (27) closely match the numerical solutions for the vertical profile of dissolved phase concentration (b) and primary mineral remaining (c). Here, we have set q_x so that $H = 10$ m for the base case parameters. The "width" of the front 2δ is the approximate distance over which C and M are changing, so long as they are not affected by the boundary condition. The circular marker in each plot gives the location of the inflection point z_w, where the profile is changing most rapidly

is changing rapidly over the 2δ thickness of the weathering front. The approximate solution is based on the assumption of a constant $-q_z^*$, and so cannot capture the behaviour as accurately there.

The results show that the relative location of the weathering front within the aquifer (z_w/H) where the $w = \omega$ condition is satisfied is largely controlled by the dimensionless ratio $\omega\eta/r$. The $\omega\eta/r$ ratio captures the effects of recharge rate, mineral solubility, and incision rate. Values closer to 1 imply lower solubility, higher incision rates, and lower recharge rates. Values closer to 0 imply the opposite. Equation 27 shows that the thickness of the weathering zone (which is around 2δ) as a proportion of the total thickness H varies inversely with a Damkhöler number $kH/4\omega$ that depends on stream incision and reaction rates. For large $kH/4\omega$, the weathering front is a sharp transition, whereas for small $kH/4\omega$, it is a gradual change over the thickness of the aquifer.

When the weathering front is close to the boundary (i.e., when $\omega\eta/r \lessapprox 0 + 4\omega/(kH)$ and/or $\omega\eta/r \gtrsim 1 - 4\omega/(kH)$), the boundary conditions have some influence on the location z_w through the term $(1 - S(H))/S(0)$. The region where the boundary conditions might have an influence is shaded grey in Figure 2. The reaction rate k only affects the location of the weathering front z_w through these terms due to its influence on δ. This influence can be seen in Figure 2a in the deviation of z_w/H from $\omega\eta/r$ in the shaded region.

This suggests that we can distinguish between two types of profiles: a *completely submerged profile* where weathering is largely complete below $z = H$ and an *incompletely submerged profile* where residual weatherable mineral reaches the top of the saturated zone. In the first case, the location of z_w is only determined by the need to find the "goldilocks" level $z_w/H = \omega\eta/r$ at which the solute transport rate matches the rock supply rate, and $2\delta = 4\omega/k$. In the second case, the proximity to the upper boundary does have an effect on z_w and δ, and some portion of the weathering of M occurs in the unsaturated zone, and/or M is removed by erosion (both of which occur outside the domain of the model developed here). These can be distinguished quantitatively by $\omega\eta/r \gtrsim +4\omega/(kH) < 1$ and $\omega\eta/r \gtrsim +4\omega/(kH) > 1$, respectively. Similar concepts and terminology have been suggested by Bazilevskaya et al. (2012) to distinguish regimes in which weatherable mineral is completely removed in the subsurface or reaches the surface, where they are also referred to as "local equilibrium" and "kinetic limitation" regimes. Here, there is no direct connection to surface erosion though, because H is the top of the saturated zone, not the ground surface (though it may be colocated with it), and the rate of advance is set by stream incision.

3.3 | Lateral flow—thin weathering zone approximation

So what happens when the weathering does increase porosity and permeability? Higher K in (13) means that q_z^* declines faster, as more water is partitioned to lateral flow (per unit increment of depth). Under the steady-state assumptions used here, this will *not* mean less water reaches the weathering zone but rather that the thickness of the saturated zone above a completely submerged weathering zone will be less. As shown above, the location of the weathering front is determined such that the "right" amount of flow passes through it to remove the weathering products. All excess recharge is diverted laterally above the weathering front. If the amount of flow passing through the weathering front were to decline, the rate of weathering front advance would decline relative to the rate of stream incision, and the front would "rise up" the profile (in a relative, not absolute, sense) until it captured sufficient vertical flux to propagate at the required rate, or for M to be removed by erosion.

Consequently, only the increase in permeability that occurs within the weathering zone can have any affect on the position of the weathering front z_w or thickness 2δ. One can imagine a limiting case in which the weathering zone is relatively "thin" (small 2δ) such that the amount of lateral flow that occurs within it is relatively small, even with the increased permeability. In that case, the vertical flux through the weathering zone (which is responsible for carrying away weathering products) will be determined by the ability of the aquifer *below* the weathering zone to drain the water laterally.

If that is the case, we can essentially ignore the weathering zone thickness and simply try to determine the thickness of aquifer below the weathering zone necessary to drain the weathering front at the required rate. That rate will be $-q_z^* = \omega\eta$, because we do not need to consider the effect of any boundary conditions on the flow. If that rate of vertical flow holds across the length of the hillslope, then it must balance the rate of lateral flow at any location x, so $-q_z^* x = K_0 z_w |\nabla h|$, where K_0 is the hydraulic conductivity of the rock below the weathering zone. This can be solved to give

$$z_w = \frac{x\eta\omega}{K_0|\Delta h|}, \tag{28}$$

which is independent of the recharge rate r and H. This expression suggests that the position of the weathering front in this case is determined largely by the hydraulic properties of the rock *below* the weathering front, not above it.

3.4 | Lateral flow—thick weathering zone approximation

We can also attempt to develop insights for the case where the thickness weathering zone cannot be neglected, and lateral flow along the weathering zone itself is an important pathway by which weathering products exit the hillslope. This may be the case if the weathering front is very gradual, or when the permeability of the unweathered bedrock is very low.

To do this, we will divide the aquifer into three zones (below, above, and within the weathering zone) and construct coupled water and solute mass balance equations for each by integrating the governing equations vertically over the zones. To solve the resulting integrals, we will assume that C and M are constant above and below the weathering zones and vary linearly within the weathering zone. For a completely submerged weathering zone, C and M will be assumed to vary at a rate proportional to $1/(2\delta)$. When the weathering zone is not completely submerged, C will be allowed to vary at a rate that ensures the boundary condition $C(H) = C^H$ is satisfied.

The mass balance equations are presented here, whereas additional details can be found in Appendix A. The three zones are defined as the following:

- *Below the weathering zone* ($0 < z < H_p$): Here, the rock is not yet altered ($M = M^0$), and the fluid is completely equilibrated

($C = C^{eq}$), so $\phi = \phi_0$ and $K = K_0$ (the permeability of the parent rock) and the vertical flux q_z^* varies linearly.

- *Within the weathering zone* ($H_p < z < H_p + H_w$): Here, C and M are assumed to vary linearly at a rate given by $1/(2\delta)$, and so ϕ, K, and q_z^* are also varying (the latter two non-linearly). In completely submerged profiles, $H_w = 2\delta$, and the weathering front is assumed to be entirely contained within $0 < z < H$. Otherwise, H_w only refers to that portion of the weathering zone that is within the saturated zone, and H_w is some fraction f of 2δ.
- *Above the weathering zone* ($H_p + H_w < z < H_p + H_w + H_s = H$): Here, $\phi = \phi_0 + \phi_m$ and $K = K_m$ (the permeability of rock once completely weathered with respect to the mineral of interest). The thickness of this zone, H_s, is zero in incompletely submerged profiles.

The total saturated thickness is the sum of these parts:

$$H = H_p + H_w + H_s. \tag{29}$$

Water balance requires that the total recharge upslope of location x must be balanced by the lateral flux through the three zones:

$$rx = \int_0^{H_p} K_0|\Delta h|dz + \int_{H_p}^{H_p+H_w} K(z)|\Delta h|dz + \int_{H_p+H_w}^{H} K_m|\Delta h|dz. \tag{30}$$

The three terms on the right are lateral flux of water below, within, and above the weathering zone, respectively. They differ only in the lateral conductivity assumed to apply in each zone. K is constant in the first and last terms, and so these integrals can be solved trivially. The permeability within the weathering front varies however, so the integral cannot be simplified easily.

Solute mass balance requires that $nM^0\omega x$, the rate primary minerals, enter the weathering zone upslope of x, plus the solutes brought in with recharge at the top of the weathering zone $C^H rx$ balance the rate that the resulting solutes are carried away by the lateral flow below and within the weathering front. Thus,

$$nM^0\omega x + C^H rx = \int_0^{H_p} C^{eq}K_0|\Delta h|dz + \int_{H_p}^{H_p+H_w} C(z)K(z)|\Delta h|dz. \tag{31}$$

Here, the first term, representing lateral export of solutes below the weathering zone, is again trivial to integrate, because the integrand is constant. However, in the second integral, both K and C vary in the vertical.

In addition to these mass balance constraints, we must also ensure that the boundary conditions are properly accounted for. This is particularly important in the case of an incompletely submerged profile. Let us call the vertical flux at z_w as $-q_w$. We will assume that (20) and (21) apply (with $-q_z^* \to -q_w$) so

$$-q_w = \eta\omega\frac{1 - S(H)}{S(0)}, \tag{32}$$

$$\delta = \frac{2w}{k} \times \frac{C^{eq} - S(H)C^{eq}}{C^{eq} - C^H}. \tag{33}$$

This vertical flux of water through z_w must be equal to lateral flux below z_w:

$$-q_w x = \int_0^{H_p} K_0|\Delta h|dz + \int_{H_p}^{z_w} K(z)|\Delta h|dz. \tag{34}$$

Equations (29)–(34) are a sufficient set of constraints to determine the values of H, H_p, H_w, H_s, z_w, and δ and will be referred to as the *thick weathering zone approximation*. Appendix A gives an iterative method for doing so that involves linearizing the variations in C and M within the weathering zone.

This set of equations can be simplified in the case of a completely submerged profile. In that case, we can assume $H_w = 2\delta$, $S(H) = 0$, $S(0) = 1$, $z_w = H_p + H_w/2$, and the size of H_s is immaterial. Equations (31)–(34) are then sufficient to characterize the system (using the same linearization method to handle the integrals, as given in Appendix A). These equations can be combined to give a simpler form of (31):

$$\eta\omega x = \left(z_w - \frac{2\omega}{k}\right)K_0|\Delta h| + \frac{4\omega}{k}K_m F_C^*|\Delta h|, \tag{35}$$

where F_C^* is a constant that accounts for the variations in K and C in the weathering zone. F_C^* decreases with larger K_m/K_0. When K does not vary with M, $F_C^* = 0.5$, and for the base case parameters (for which weathering increases permeability by a factor of 6), $F_C^* \approx 0.2$. In the limit of a completely impermeable bedrock (i.e., $K_0 = 0$), $F_C^* = 1/20$.

This equation captures the balance that must be struck between permeability, lateral hydraulic gradients, solubility, and reaction rates when the unweathered bedrock is impermeable and diffusion can be neglected. It reduces to (28) when ω/k is small, as we would expect. However, when $K_0 = 0$, we see that all terms with z_w disappear, and ω cancels, leaving

$$|\Delta h| = \frac{k\eta x}{4K_m F_C^*}. \tag{36}$$

This implies that in the limit where lateral flow along the weathering zone dominates, the weathering front elevation z_w is not determined by the model laid out so far. As we shall see in Section 5 though, it can be determined by the constraint (36) places on the hydraulic gradient $|\nabla h|$.

3.5 | Comparison with numerical solutions

The thick and thin weathering zone approximations given were evaluated and compared with numerical solutions for the base case parameters. Several parameters were also varied to explore the sensitivity of the solutions and illustrate insights gained from the analytical approximations. The results are shown in Figure 3.

For the parameter sets explored, the thick weathering zone approximation (dashed line) matches the numerical result very closely in all cases apart from those where the thickness of the weathering zone approaches the saturated thickness (e.g., the case with the smallest k^s). The deviation in those cases can be attributed to the large change in the vertical flux rate across the weathering zone, in violation of the assumptions.

The thin weathering zone approximation tends to overestimate the location of z_w obtained from the numerical solution (solid line). Unsur-

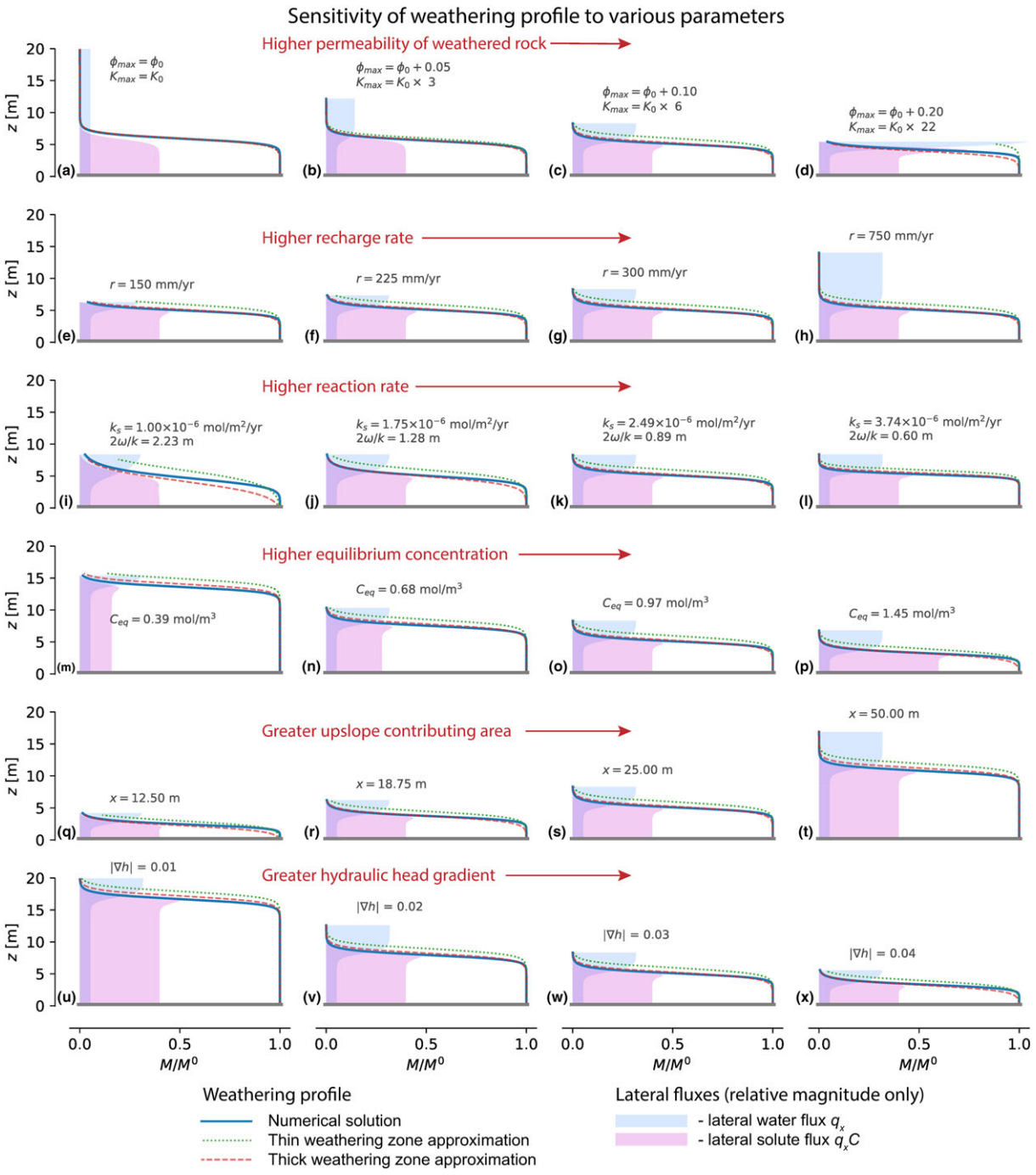

FIGURE 3 Sensitivity of the profile of primary mineral content M to various factors. The third column of plots above (plots c, g, k, etc.) represents the vertical profile at a distance of 25 m from the groundwater divide for the base case parameters (see Table 1). (a–d) Varying the permeability of the weathered rock (by varying the final porosity of the weathered rock) has only a small effect on the weathering front location z_w, and varying the recharge rate (e–h) has almost no effect. (i–l) The reaction rate modifies the thickness of the weathering zone, but not its location. (m–p) The solubility of the rock, however, has a strong effect, as does the distance downslope from the divide (q–t) and hydraulic head gradient (u–x)

prisingly, it does better for larger k (plot l), which gives a thinner weathering zone. More surprisingly perhaps, it is nearly exactly right for the case where weathering does not affect the permeability (plot a) but becomes increasingly inaccurate as weathered permeability increases. This can be understood by considering the thick approximation Equation 36. When $K_0 = K_m$, the factor F_C^* that accounts for the vertical variation in lateral flow through the weathering zone equals 0.5. This causes the term accounting for front lateral flow within the weathering front to exactly cancel the $-2\omega/k$ part of the term accounting for lateral flow below the weathering front. The resulting equation can be rearranged to yield an expression identical to the thin weathering zone approximation (28).

The relatively small difference between the thin approximation and the numerical results suggests that in the cases examined here, the porosity–permeability feedbacks are not critical in controlling the position of the weathering front. The reason why it can be seen by considering the vertical distribution of water and solute mass fluxes moving laterally, as shown by the pink and blue shaded regions in

Figure 3. In most cases, the majority of the water flux exits the system above the weathering front and consequently has a low concentration of weathering products. The water below the weathering front is saturated in weathering products and carries away the majority of the weathered mass, despite being a much smaller flux of water. The lateral flux of weathered solutes within the weathering zone is greater than the lateral flux below *per unit vertical distance* because of the porosity–permeability feedbacks, but the limited thickness of the weathering zone means that contribution of this to the total solute flux is relatively small.

This explains the sensitivity of the weathering front to the parameters shown in Figure 3. Increasing the permeability of the weathered rock does drive the weathering front slightly deeper, but the effect is not very great, even over a 22-fold change in K_m. The lateral flux of weathering products in the higher permeability material is still small compared with the vertical flux into the unweathered zone. Changing the recharge rate r has no apparent effect at all, as the extra water moves laterally above the weathering front and does not carry away extra solutes. Changing the reaction rate k^* alters the thickness of the weathering front but not the location.

Two of the parameters varied in Figure 3 relate to the location of the vertical profile considered in the context of the hillslope as a whole: x and $|\nabla h|$. As the distance downslope from the ridge x is increased, more flow must be transported from upslope and so the thickness of the aquifer below the weathering front must increase. Alternatively, if the hydraulic gradient $|\nabla h|$ is decreased, the saturated thickness must increase to compensate. However, $|\nabla h|$ varies in x due to variations in the elevation of the impermeable base B and the saturated thickness H. And the saturated thickness H is itself determined by the model presented here.

This means that when considered in the context of the hillslope, $|\nabla h|$ is not a free variable but rather must be determined along with the other parameters. This point will be returned to in section 5. First though, we must consider the role of diffusion.

4 | INSIGHTS FROM ANALYTICAL SOLUTIONS (ADVECTION AND DIFFUSION)

4.1 | Advective versus diffusive transport

The above numerical model and analytical solutions are derived under the assumption that advection dominates the transport of weathering products away from the weathering front. What happens if diffusion dominates instead? When is this likely to be the case?

Analytical solutions that incorporate both diffusion and advection are not available. However, we can estimate the potential importance of diffusion by calculating a Peclet number for the weathering zone. The Peclet number is the ratio of the rate of advection to the rate of diffusion. The advection rate is set by the pore fluid velocity q_z^*/ϕ. The diffusion rate declines with distance as $2D_m/\Delta z$. The relevant Δz is the thickness of the reaction zone H_w.

We can use the results derived above for a completely submerged profile to obtain a first-order estimate of the flow rate and thickness of the reaction zone in the absence of diffusion and use the calculated Peclet number to determine whether the assumption that diffusion is negligible can be ignored. If we find that Pe $\gg 1$ or even Pe~ 1 it is unlikely that diffusion affects the location or thickness of the weathering front. However, if Pe $\ll 1$, this cannot be said. Thus, setting $\Delta z = 2\delta = 4\omega/k$, and $-q_z^* = \omega\eta$. This gives

$$\mathrm{Pe} = \frac{2\eta\omega^2}{kD_m\phi}. \tag{37}$$

This implies that (assuming weathering keeps pace with the rate of incision) the relevance of vertical diffusion within the weathering zone varies with the square of the incision/rock supply rate, ω^2. Advection dominates when incision is rapid, whereas diffusion dominates when it is not. For the base case parameters (with $\phi = \phi_0$), we have Pe= 14.8. This suggests advection dominates in the base case parameters. We might expect that a numerical solution that includes diffusion would deviate only slightly from the solution provided above as a result.

4.2 | Weathering of an impermeable bedrock by diffusion

When the permeability of the bedrock is very small, diffusion may be the only way weathering products can be transported away from the weathering front. Advection laterally through the weathering zone is possible, but this is only capable of carrying away sufficient solutes to keep up with incision if the weathering zone is sufficiently thick.

Is it possible for diffusion upwards from the weathering front (i.e., against the direction of vertical advective flow) to drive sufficient weathering products into the into the overlying aquifer and then out of the system? Here, we will consider this case and attempt to derive a relationship between diffusive transport and the rock supply rate. Let us assume that the thickness of the weathering zone is relatively small, and so lateral flow along the weathering front itself can be neglected. Consequently, all lateral flow is in the saturated zone above the weathering zone (H_s, as defined above). Therefore, we will set $z = 0$ at the weathering front, and let $K = K_m$ throughout (i.e., permeability is homogeneous). The vertical flux rate in this case declines linearly with depth as $-q_z^* = rz/H(x) = zK_m|\Delta h|/x$. The weathering reaction is assumed to occur only at this lower boundary, where it maintains the concentration at equilibrium. This is represented by the boundary condition $C(x,0) = C^{eq}$ at $z = 0$. Equation 1 then has a solution:

$$C(x,z) = C^{eq}\left(1 - \gamma\ \mathrm{Erf}\quad\left(\frac{z}{H_D(x)}\right)\right), \tag{38}$$

where Erf() is the error function, H_D defined as

$$H_D(x) = \sqrt{\frac{2D_m x\phi}{K_m|\Delta h|}}, \tag{39}$$

and γ is a value that depends on H_D and H (see Appendix A). We have neglected the terms arising from transforming (1) into a moving frame of reference, which are small when ω is small relative to r/ϕ, and would disappear in later results anyway.

The variable γ accounts for the constraint that diffused solutes are removed laterally within a distance $H(x)$, and varies approximately as $\gamma \approx 1 - e^{-H/H_D}$. This converges rapidly to 1 if $H > H_D$ (i.e., when the

back-diffusing solutes are not limited by the thickness of H). This will be assumed to be the case for subsequent results.

The weathering front advance rate can be obtained by setting the supply of weatherable minerals equal to the rate of removal of weathering products from the weathering front by diffusion, so

$$nM\omega = -\phi D_m \left.\frac{\partial C}{\partial z}\right|_{z=0}, \tag{40}$$

$$\text{so} \quad \eta\omega = \frac{2D_m\phi}{H_D\sqrt{\pi}}. \tag{41}$$

Substituting the definition of H_D (39) and rearranging then gives us

$$\eta\omega = \sqrt{\frac{2D_m\phi K_m|\Delta h|}{\pi x}}. \tag{42}$$

This provides an expression for the diffusion-dominated case that is analogous to (35) for the advection-dominated case.

5 | THREE MODES OF HILLSLOPE-SCALE FEEDBACK BETWEEN LATERAL FLOW AND WEATHERING

Equations 35 and 42 describe the essential balance between the supply of fresh rock to the weathering zone in a hillslope and the capacity of the hillslope to transport the resulting weathering products away through lateral flow. The head gradient $|\Delta h|$ appears in each of these and has been treated up to now as a fixed parameter. However, it is a gradient that arises from the broader context of the hillslope and the valley to which it is draining. It is therefore as much a consequence of the coevolved hillslope structure as it is a driver of that coevolution. Here, we will consider this gradient and the hillslope architecture implied by it in several cases.

From the analysis so far, we can distinguish three "end-member" configurations of hillslopes implied by Equations 35 and 42 (see Figure 4):

- **Diffusing up**. Parent rock permeability is low and the weathering zone is thin—consequently, advection alone is not capable of removing weathering products. Instead, they diffuse back up into the aquifer above the weathering zone, where lateral flow is sufficient to remove them at the required rate. In this case, (42) applies.
- **Draining down**. The permeability of the parent rock K_0 is sufficiently large (perhaps due to fracturing) that deep drainage vertically through the weathering front carries the great majority of weathering products away. In this case, the last term in (35) can be neglected, so that (28) applies.
- **Draining along**. Although the permeability of the parent rock is low (effectively zero), weathering is able to increase permeability sufficiently for lateral drainage within the weathering zone itself to remove the weathering products. In this case, we neglect the first term in (35), so that (36) applies.

These three possibilities each imply a different relationship between ω and $|\nabla h|$. Here, we will explore these relationships in order to extend the 1-D analysis presented above to a 2-D slice of a hillslope. We will also determine the maximum relief of the bedrock, which is to say,

$$\text{Relief} = H_p(0) - H_p(L). \tag{43}$$

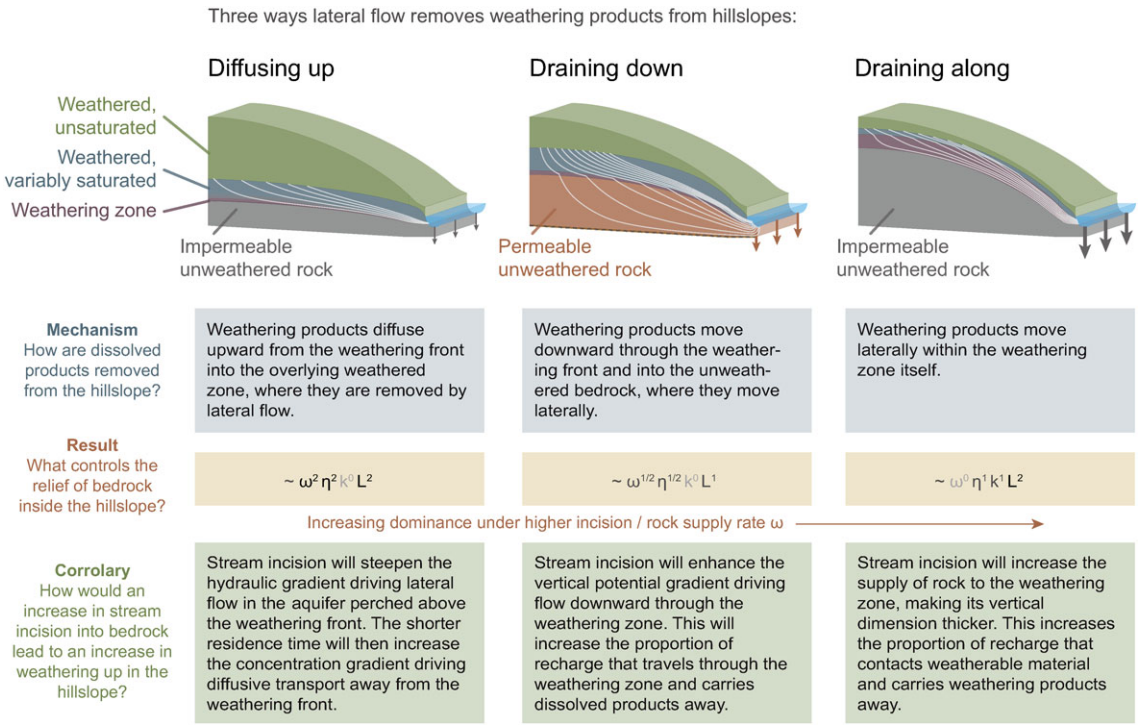

FIGURE 4 Three ways lateral flow removes weathering products from hillslopes. Each transmits the solutes in a different primary direction, has a different dependence of bedrock relief on the driving factors (stream incision rate ω, resistance to dissolution η, reaction rate k, and hillslope length L), and responds differently to an increase in stream incision (rock supply) rates

This is not the relief of the surface topography, but it does put a lower bound on the surface topographic relief.

5.1 | Draining down

In the draining down case, we might assume that K_m/K_0 is sufficiently large that the thickness of the overlying aquifer H_s is relatively small, and the gradient of the bedrock–saprolite interface H_p provides the primary hydraulic gradient driving flow in the system. If we assume that the gradient of the impermeable boundary B is small (so that the requirements laid out in Harman and Kim (2018) are met) then $\Delta h \approx \nabla H_p = dH_p/dx$. This means we may treat the unweathered bedrock itself as a hydraulic groundwater aquifer with recharge rate $\eta\omega$, and we can simply use the analytical solution for this case (Equation 12 of the companion paper, Harman and Kim, 2018) to predict its upper elevation H_p:

$$H_p(x) = \sqrt{H_{bp}^2 + \frac{\eta\omega}{K_0}\left(L^2 - x^2\right)}, \tag{44}$$

where H_{bp} is specifically the thickness of the permeable unweathered bedrock at $x = L$, rather than the saturated thickness. We can then obtain the elevation of the weathering front as $z_w = H_p + \delta$. Using this equation, the hydraulic gradient at a location x downslope of the divide can be approximated as

$$|\Delta h| = \frac{x\eta\omega}{K_0 H_p(x)}. \tag{45}$$

Note that this equation is entirely independent of the recharge rate r and the conductivity of the weathered rock, and z_w is only dependent on reaction rate k through the δ term.

This simple approximation of the weathering front elevation is very similar to that suggested previously by Rempe and Dietrich (2014). Indeed, Equation 44 is almost identical to their Equation 3, with two differences. First, where (44) has the term η, Rempe and Dietrich

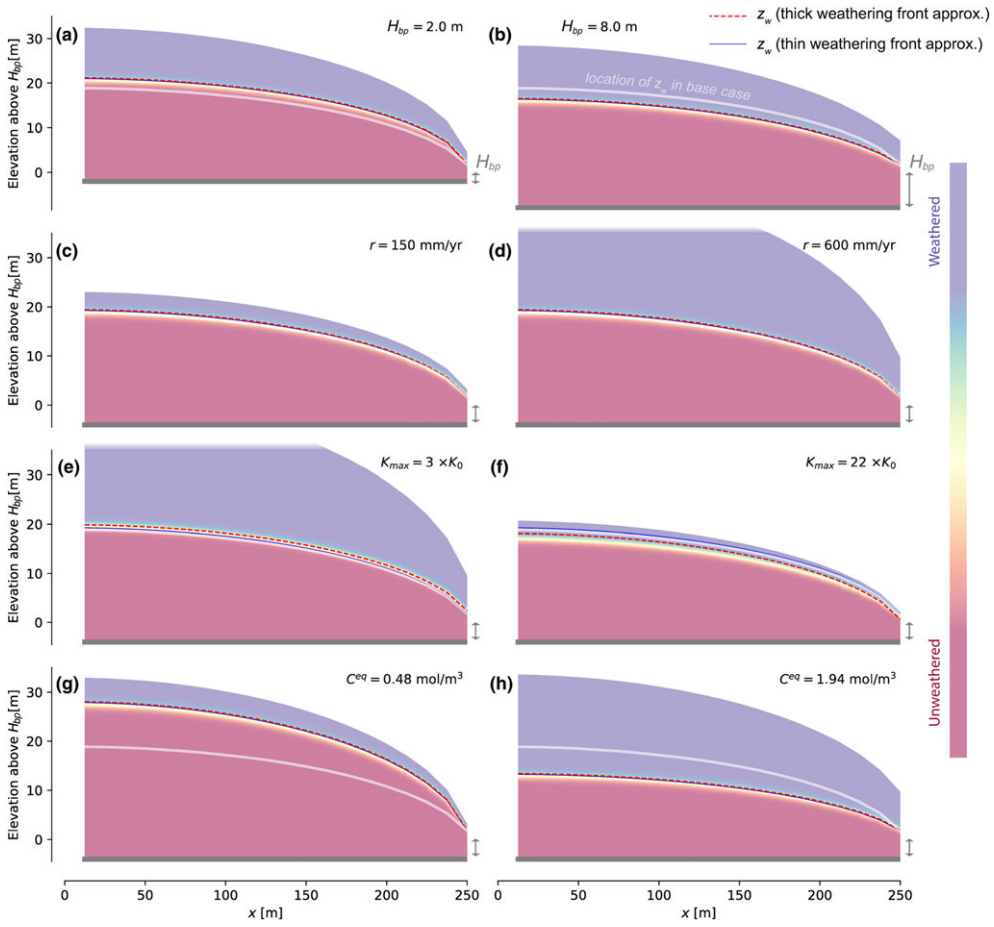

FIGURE 5 (a) Relationship between rock supply rate (i.e., the rate of stream incision) and bedrock relief required to export weathering products from the hillslope at a matching rate, assuming base case parameters (representative of plagioclase feldspar weathering in a humid climate). Each of the three mechanisms requires a different relief—in a situation where all three might be operating, we would expect the one that requires the least relief to determine the actual relief. Here, because the bedrock is slightly permeable ($K_0 = 11$ m year^{-1}), the "draining down" requires the least relief over the realistic range of rock supply rates. "Diffusing up" dominates only for very low incision rates, and "draining along" only for very high incision rates (and anyway would have a hillslope number Hi> 1, violating the assumptions of the model). The "draining down" result is sensitive to the thickness of parent rock at the downslope boundary through which water can exit the hillslope (H_{bp}, dotted red lines). The model is not technically valid in the grey area, as the assumed recharge rate r is not sufficient to remove weathering products at the rate required to keep up with rock supplied by channel incision $\omega\eta$. Rock would need to be removed by physical erosion in those cases.) (b–d) The sensitivity to modifying various parameters by factors of 1/25, 1/5, 5, and 25. (e,f) The effect of ω on the thickness of the weathering zone 2δ, and the weathering zone Peclet number. (g) The distribution of 482 observed basin-scale erosion rates for temperate climates reported in Portenga and Bierman (2011)

(2014) has porosity ϕ. This difference reflects the different arguments used to derive the models. Rempe and Dietrich (2014) derived their model based on the assumption that weathering is initiated when the original formation water of the rock (occupying the initial porosity ϕ) has been removed and replaced with reactive water or air. Under the "draining down" scenario, the unweathered bedrock must be flushed with approximately η pore volumes of reactive water before weathering is complete. For our base case parameters, $\eta = 2612$. Second, Rempe and Dietrich (2014) set the H_{bp} to zero in order to determine an upper bound on bedrock relief. As Figure 6 shows, this thickness has a moderate control on the required relief, and we therefore include the case where $H_{bp} > 0$.

Figure 5 shows the effect of varying several parameters in the draining down case. The slope used in the numerical solution at each x is the slope implied by (45). Note that the surface elevation is not shown here and has not entered into our calculations.

The results show that (44) is a good match to the numerical solution for z_w. As implied by the analytical approximation, varying the recharge rate has no effect on the elevation of the weathering front, only on the thickness of the aquifer above. The effect of varying the permeability of the weathered rock is also small. The largest effect comes from varying $\eta\omega/K_0$. The toe boundary condition H_b also has an effect on the position of the weathering front.

The maximum relief of bedrock at the ridge relative to bedrock at the toe can be written as

$$\text{Relief}_{deep} = L\sqrt{\frac{\eta\omega}{K_0}}\sqrt{\frac{H_b^2 K_0}{L^2\eta\omega} + 1} - H_{bp}, \tag{46}$$

where the $-H_{bp}$ is included so relief is measured relative to the top of the parent bedrock (rather than from B) at the toe of the hillslope. This result implies that the relief necessary to sustain weathering by deep drainage varies with the rock supply rate as $\omega^{1/2}$.

5.2 | Draining along

For the "draining along" case, the thickness of the flow carrying weathering products is the weathering zone itself $H_w = 2\delta = 4\omega/k$, as $K_0 \sim 0$. This also implies $F_C^* = 1/20$. Assuming a completely submerged profile, Equation 36 gives a relationship between $|\nabla h|$ and x, whereas (30) can also be used to determine an equation for H_s (see Appendix A):

$$H_s = \frac{r - 5\eta\omega}{5k\eta}. \tag{47}$$

This equation demonstrates that H_s is invariant in x, because everything on the right of the equation is constant. Consequently, $H_w'(x) + H_s'(x) = 0$, and so the potential gradient must be provided by the bedrock gradient. Therefore, we must have $|\Delta h| = -H_p'(x)$. Inserting this into (36) and integrating (assuming $H_p(L) = 0$), we can obtain

$$H_p(x) = \frac{5k\eta}{K_m}(L^2 - x^2), \tag{48}$$

which implies that the maximum relief in this case is

$$\text{Relief}_{lat} = \frac{5L^2 k\eta}{K_m}. \tag{49}$$

This relationship is independent of ω. Increases in the rock supply rate in this case do not require changes in the relief of the hillslope but only in the thickness of the weathering zone.

5.3 | Diffusing up

For the "diffusing up" regime, we can rewrite (42) as

$$q_x(x) = x\frac{\pi\eta^2\omega^2}{2D_m\phi}. \tag{50}$$

This equation suggests that the lateral flow rate must increase linearly downslope. For this to occur under spatially uniform recharge, the thickness of the flow must be constant, so as before $H_w'(x) + H_s'(x) = 0$. Combining the equation above with (3), setting $|\nabla h| = -H_p'(x)$, and integrating, we can obtain

$$H_p(x) = \frac{\pi\eta^2\omega^2}{4D_m\phi K_m}(L^2 - x^2), \tag{51}$$

and so total relief is

$$\text{Relief}_{diff} = \frac{\pi L^2\eta^2\omega^2}{4D_m\phi K_m}. \tag{52}$$

This suggests that when back-diffusion balances weathering rates the relief varies with ω^2.

5.4 | Synthesis of the three modes, and the principle of least relief

Figure 6a shows the relief required for the base case (plagioclase feldspar weathered with 300 mm year^{-1} of recharge; see Table 1) if the rate of rock supply by channel incision ω is varied. Figure 6g shows the distribution of basin erosion rates from temperate regions measured using ^{10}Be, as reported by Portenga and Bierman (2011). Most are within the range of 1–10,000 m million year^{-1}.

The "diffusing up" mode requires very little bedrock relief to export weathering products when ω is very small, but the required relief increases rapidly, and for the rate used in Section 3 above (ω = 30 m million year^{-1}) reaches around 600 m (over a 250-m-long hillslope). For $\omega > 5$ m million year^{-1}, the relief is enough that $Hi > 1$, which means the assumption of scaled lateral symmetry may be violated in those cases.

The relief required by the "draining down" mode increases more slowly than "diffusing up" mode ($\omega^{1/2}$ rather than ω^2) and is less for all $\omega > 2$ m million year^{-1}. For the base case, "draining down" requires relief of about 20 m. The result is somewhat sensitive to the thickness H_{bp} through which water can exit the hillslope—Less relief is required when the thickness of permeable parent rock is larger. Advection is faster at transporting solutes through the weathering zone only once $\omega > 20$ m million year^{-1}, so it is possible that for slower incision, rates diffusion has additional effects on the shape of the weathering zone even while weathering products are removed by downward advection.

The relief required by the "draining along" mode is insensitive to the incision rate and is always around 420 m (and Hi > 1). However, as the sensitivity analysis in Figure 6 shows, that value is sensitive to hillslope length, solubility, and (uniquely of the three mechanisms) reaction rate k.

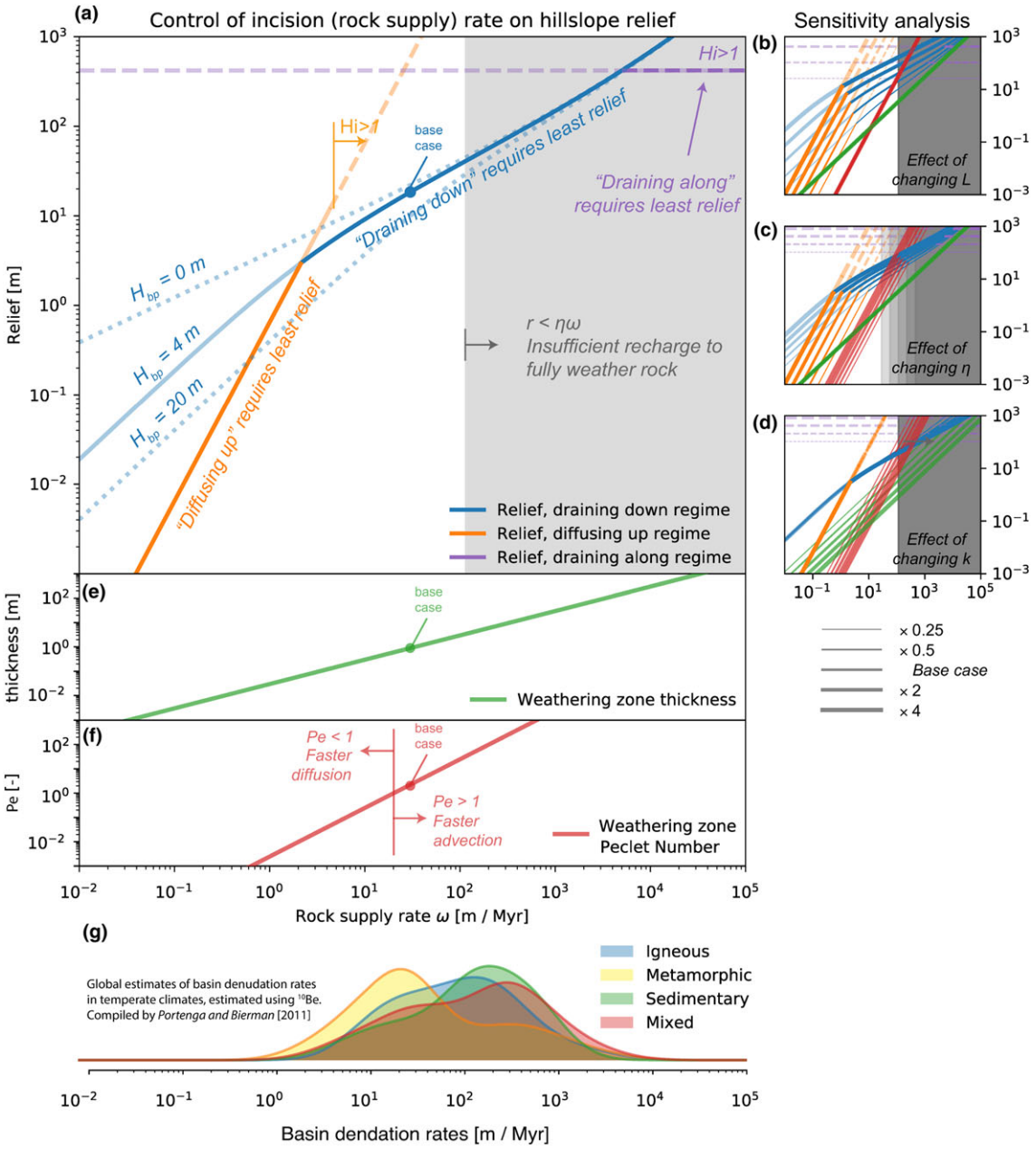

FIGURE 6 Sensitivity of a hillslope in the "draining down" mode to variations in the parameters around the base case. The slope of H_p implied by Equation 44 was used to set Δh for the numerical and approximate solutions. The gradient colours are interpolated from the 1-D numerical solution evaluated at a range of x locations. Estimates of z_w from the thick and thin weathering front approximations are given with red dashed and blue dotted lines. The thick weathering front approximation for z_w with base case parameters is shown in the lighter coloured line for comparison. The note that the upper parts of the profiles in plots (d) and (e) extend above the axis range

So which of these three mechanisms will actually dominate in any given scenario? If we constructed a model that includes all the processes that contribute to these export mechanisms, we would likely find that the one that requires the least relief to export the solutes at the rate required by rock supply would in fact dominate and would set the steady-state relief. If the higher relief required by the other mechanisms was imposed as an initial condition in the model, the "least relief" mechanism would inevitably export solute at a rate higher than ω and thus lower the bedrock relief toward its own limiting required rate.

This reasoning makes it unlikely that the "diffusing up" mechanism is significant for plagioclase feldspar dissolution. Few landscapes have $\omega < 2$ m million year^{-1}, and all are deserts where hillslopes are unlikely to have a persistent saturated zone draining to adjacent streams. The sensitivity analysis suggests that "diffusing up" may be significant for more soluble minerals in slowly eroding landscapes.

The "draining along" mechanism also seems unlikely to be significant within the range of conditions captured by the model assumptions. However, if the reaction rate k were substantially slower (so that the weathering zone is thicker than the 1.8 m of the base case considered here), it may be significant in areas where the unweathered rock is relatively impermeable.

Equations describing the "draining down" mode were derived under the assumption that the effects of diffusion can be neglected. How-

ever, Figure 6f shows that the weathering front Peclet number is less than 1 for a wide range of realistic ω. Within these cases, we would expect the effects of diffusion to modify the shape of the weathering profile, but it is not clear whether diffusion would substantially modify the pathway by which weathering products are exported.

Strictly speaking, the results shown in Figure 6 are only valid for where the recharge is in excess of the that required to remove weathering products at the rate required by ω, that is, $r > \eta\omega$. The region where this assumption is violated for the base case parameters is shown in grey in Figure 6a—about half the Portenga and Bierman (2011) observations fall in the invalid region under the base case parameters. In those cases, we would expect that weathering occurs primarily in the freely draining unsaturated portion of the hillslope and/or that much of the primary mineral survives to the upper part of the regolith where it must be removed by erosion.

6 | DISCUSSION

6.1 | Weathering, lateral flow, and coevolution

The model presented here can be seen as an elaboration of the hypothesis presented by Brantley et al. (2017) that weathering fronts and lateral flow pathways are mutually adjusted within hillslopes such that weathering products are exported at the rate required to keep pace with stream incision. It also provides a possible explanation for the observation that in systems with permeable bedrock, weathering fronts in the subsurface tend to be nested with the most soluble products removed at depth, and the least soluble higher up (Brantley, Holleran, Jin, & Bazilevskaya, 2013). This outcome is directly predicted by Equation 26, which suggests a proportionality between weathering front elevation z_w and η (which varies inversely with solubility). It also demonstrates the circumstances under which a mechanism for coupling weathering to stream incision similar to that suggested by Rempe and Dietrich (2014) could arise.

These results suggest mechanisms by which hillslopes' hydrologic structure may arise from the coevolution of water flow and geochemical reactions. Beyond insights into the evolution of the critical zone, an understanding of coevolved hydrologic flow paths adapted to the dictates of geochemical and geomorphic processes is of interest to those pursuing a "Darwinian" sort of understanding of hydrologic science (Harman & Troch, 2014). It offers hope that the unknown properties of the landscape controlling hydrologic function (the storage and release of water to a stream) are explicable, and potentially predictable, in terms of the long-term evolution of the system.

The potential importance of H_{bp} examined in Section 5 highlights the importance of understanding the physical meaning of B if the "draining down" mode is actually operating in a real-world case, because H_{bp} is nothing more than the depth of B below the weathering zone at the hillslope toe. The alternative origins discussed in Section 2.2 all imply a connection between surface processes and topography and the deepest extent of meteoric water circulation, with implications for everything that happens in between. Future work might investigate the feedbacks that arise from this interaction.

6.2 | Simplified models as a baseline for understanding complexity and framing hypotheses

The simplified model presented here could be tested against empirical data by examining whether the relationships underlying Figure 6 predict variations in the elevation of important weathering fronts between hillslopes with similar geological settings but differing rates of overall erosion. Where data on the weathering front elevations are not available, curves like those in Figure 6 might predict the lower envelope of overall landscape relief. However, it would be necessary to determine the hydraulic conductivity of the hillslope material (a difficult proposition) or assume that it does not vary significantly (which is dubious).

It may be more useful though as a baseline for understanding the role of lateral flow processes in more complex situations. The quantitative relationships presented here could be useful for those attempting to model weathering and lateral flow processes using more sophisticated spatially explicit numerical models (Li et al., 2017). We would expect that a model constructed with assumptions similar to our simpler model (or in such a way that the assumptions are not violated) would produce results that are in agreement with it. Our model should anticipate the relief and dominant solute export pathway of more complex models over a range of stream incision rates.

However, the insights that have been gleaned so far from the model allow us to speculate a little on what the effect might be of relaxing various model assumptions. These speculations amount to hypotheses that might be tested either through data or more detailed numerical modeling.

6.2.1 | Geochemical complexity

The model presented here is built on the type of simplified kinetic rock weathering models extensively explored in the geochemistry literature (e.g., Lebedeva et al., 2010; Li et al., 2014; Maher, 2011). This model is analytically tractable and can be parameterized based on measured parameter values. However, it does not do justice to the full complexity of chemical weathering reactions. Weathering is not simply the dissolution of one species and the production of another. It typically involves multiple components being consumed and produced concurrently and in sequence.

Even so, insights from the analysis above can be applied to understand how more complex reaction sequences play out in hillslopes. Reactions may be limited not only by the saturation of the fluid by some dissolved species (as has been assumed here) but by the consumption of important species carried in with the recharge (e.g., acidity in acid-base weathering reactions or electron receptors in oxidation reactions). In that case, it may be that the supply of these species determines the depth of the weathering front. If so, the partitioning of flow laterally is still an important consideration, because it represents a loss of unreacted species from the system. This loss will limit the supply in the reaction zone, creating the (perhaps paradoxical) situation whereby the overall reaction rate is limited by the availability of some species that seems abundant in the lateral outflow from the hillslope. In that case, the vertical location of the weathering front (at dynamic steady state) will presumably still be such that the supply of the reactive species with percolating recharge is just sufficient for the

weathering front advance rate to keep up with the rate of channel incision.

6.2.2 | Fine-scale heterogeneity and the efficiency of the "draining along" mode

The simplified kinetic rock weathering model employs the implicit assumption that the weathering rock can be treated locally as a homogeneous and well-mixed porous medium. Where this assumption is violated, there may be differences between local parameters and the "effective" parameters that determine the larger scale behaviour. For example, the value of reaction rate k used in the base case may be substantially larger than that required to reproduce hillslope-scale processes. Recent work (Jung and Navarre-sitchler, 2018a, 2018b) has demonstrated that fine-scale heterogeneity in permeability can have significant effects on apparent values of effective weathering reaction rates k, perhaps accounting for well-documented reduction in reaction rates over time. Weathering proceeds first along fast flow paths where the small effective porosity means weathering products can be rapidly removed by advection. Once primary minerals are exhausted in those areas, the rate of weathering becomes limited by the rate solutes that can diffuse between the high- and low-permeability zones. This is essentially a small-scale version of the process of core-stone weathering in which weathering proceeds from fracture faces (where fluid is frequently refreshed) into the unfractured block interiors where solutes must move via diffusion (e.g., Buss, Sak, Webb, & Brantley, 2008). These processes might lead to a smaller effective k in heterogeneous weathering zones, which in turn produces a substantially larger weathering zone. This may mean that in heterogeneous material the "draining along" mode is a substantially more effective mechanism for exporting weathering products than the analysis presented above would indicate.

6.2.3 | Porosity-permeability feedbacks in weathering

The model also adopts a very simple representation of the effects of weathering on permeability. It neglects effects on pore morphology, size distribution, and connectivity and assumes that secondary precipitation occurs linearly with primary mineral dissolution. These deficiencies may not be critical though. The results above suggested that the increase in permeability with weathering did not strongly control the location or thickness of the weathering zone. If "draining down" dominates, it is only really essential to know the permeability of the unweathered rock. The results for the "diffusing up" and "draining along" cases hint that it is more important to know the relative permeability of weathered and unweathered rock than it is to know the nature of the non-linear increase between these end members. However, further work in this area is surely required.

6.2.4 | Surface erosion and vadose zone weathering

As stated, the model does not directly account for the effects of weathering in the unsaturated zone, or the effects of surface erosion. However, nothing in the formulation requires the assumption that surface erosion and weathering above the saturated zone are unimportant. Rather they will alter the conditions at the upper boundary of the model domain: the recharge r and inflow concentration C^H. These in turn will modify the value of H and the residual mineral content M^H that satisfies the boundary condition that $M = M^0$ at $z = 0$.

In effect, these boundary conditions communicate the terms of the "balance of labour" between surface erosion, weathering in the vadose zone, and weathering in the saturated zone in removing minerals from the system. The more soluble a mineral is, the deeper in the profile it is weathered, and the more completely developed its profile (Lebedeva & Brantley, 2013). Relatively insoluble minerals will survive the relatively low vertical flux rates in the saturated zone and progress to the vadose zone to be weathered there (perhaps more effectively due to the greater acidity or availability of oxidants), or to the surface to be removed by physical erosion.

Depending on the mineral considered, the degree of weathering M/M^0 of material that arrives in the upper regolith might affect the cohesion and grain size of that material and so affect the depth of soil that develops and the slope and upslope area required to transported regolith by surface erosion and mass movement (Dixon, Heimsath, & Amundson, 2009). In principle, landscape evolution models could be modified to account for these effects.

However, it may be the case that (at steady state) the surface slope required to transport colluvium and the subsurface slope required to transport weathering products are different. This will lead to variations in the depth of weathering across the hillslope, with deeper weathering at the ridge than at the hillslope toe, or vice versa. These differences may have the secondary effect of modifying the values of C^H and r across the length of the hillslope, violating the assumptions of the model as presented here. This could produce additional downslope variations in weathering processes not predicted by this simple model. It would be interesting to examine these interactions in a fully coupled model (Li et al., 2017).

6.2.5 | Transient recharge dynamics and the importance of the saprolite water retention curve

Models of geochemical weathering often assume steady-state flow, as we have here. In reality, recharge is intermittent, arriving seasonally and as pulses following precipitation and snowmelt. It is worth considering whether the event-like nature of recharge events could have a significant bearing on the weathering.

If we relax the steady-state assumption and allow recharge rates r to vary in time, one might initially expect that this will produce similar variations in the vertical flux rate q_z^* through the weathering zone, leading to variations in the overall rate of weathering. In fact, it is unlikely to be so simple. Under the assumptions adopted, the saturated aquifer is nearly hydrostatic, and so q_z^* is determined in the model by mass balance, not by vertical pressure gradients. An increase in r can be accommodated by increasing the thickness of the laterally flowing portion of the aquifer or by increasing the lateral pressure gradient so that q_x increases. The rate of vertical percolation can only increase if q_x increases. If an increase in r does not lead to an increase in the lateral pressure gradient within or below the weathering zone, then all the additional water will be released laterally above the weathering zone and will not affect the weathering front advance rate.

Therefore, it is worth asking what determines the effective extent of H in saprolite under transient conditions. As noted previously, H

should not be confused with the water table, which represents the contour of pore water at atmospheric pressure. In fact lateral flow can occur well above the water table in areas with pore pressure below atmospheric so long as the pore space remains saturated. Rather H is the transition from (predominantly) free vertical drainage (in which the vertical profile of pore water pressure is approximately constant with depth) to drainage constrained to flow laterally (in which the vertical profile of pore water pressure is approximately hydrostatic).

Consequently, it may be that the volume of saprolite in which water is flowing laterally may be less dynamic than the water table itself. Saprolite often contains fine pores that would require substantial tension to desaturate (e.g., a 1-μm pore requires about 14 m of hydraulic tension below atmospheric). In that case, the saprolite will only cease to be hydrostatic if sufficient tension is supplied by the relief of the hillslope itself or by root water uptake by plants (which can supply very substantial amounts of tension). If the saprolite remains at or near hydrostatic conditions and pores do not desaturate, fluctuations in recharge could generate rapid variations the pore pressure (and in the water table) that would lead to rapid variations in the lateral pressure gradient and therefore the vertical flow rate through the weathering zone. If the permeability is relatively low, these pressure fluctuations may not be visible in wells or may be substantially muted.

The consequence however would be a fluctuating flow rate through the saturated thickness. The importance of these fluctuations depends on the timescale over which they operate. The timescale for weathering is determined by the reaction rate and the mineral content as $\sim (kM^0)^{-1}$. This is around 4.7 years for the base case parameters. Fluctuations in the flow rate over timescales substantially less than 4.7 years (event scale and seasonal variations) would therefore have little effect on the weathering profile. Fluctuations at longer timescales (decadal-scale and longer) would presumably matter more, with the weathering zone thickness presumably reducing during periods of low flow and expanding during periods of high flow. This is consistent with observations of changes in apparent weathering rates associated with shifts in climate over several decades (Manning, Verplanck, Caine, & Todd, 2013).

Of course, this picture changes substantially in the presence of fractures and large connected pores. These can desaturate at lower tensions and may hydraulically disconnect the matrix in a block from the hillslope-scale pressure gradients. The potential transport-related effects discussed above are also separate from the any effects that would arise from temporal variability in the chemical composition or temperature of the recharge itself. The complexities that might result from either of these complications are beyond the scope of what we consider here.

7 | CONCLUSION

We have presented a simplified model of weathering within hillslopes at geomorphic steady state that captures the two-way interactions between weathering and lateral subsurface flow in hillslopes. The model couples together (a) the 2-D advection–diffusion reaction equation, simplified by the assumption of "scaled lateral symmetry" (see companion paper Harman and Kim, 2018); (b) a simplified kinetic model of rock weathering; and (c) a model of weathering's effect on porosity and permeability based on the Kozeny–Carmen equation.

The results suggest three end-member modes of solute export, which we have termed for convenience "diffusing up," "draining down," and "draining along." Each of these pathways of solute export requires a different amount of bedrock relief (elevation of bedrock under the ridge, relative to the elevation of bedrock at the hillslope toe) in order to export solutes at the rate required to keep pace with stream incision. The "principle of least relief" suggests that the pathway that requires the least relief will be the one that operates in a given scenario. For the example parameters explored here, "diffusing up" required the least relief at low incision rates, whereas "draining down" requires the least at higher rates. The "draining along" case is the least likely condition, but this mechanism may be sensitive to the presence of heterogeneity. Further study is required on this point.

The three mechanisms elaborated by this model recapituate both the conceptual models of Brantley et al. (2017) and Rempe and Dietrich (2014). They suggest a suite of ways the architecture of the critical zone might be configured to export the products of weathering of minerals with different solubilities at the pace they are supplied, as suggested by Brantley et al. (2017). One of the three configurations is a "bottom-up" control of the sort suggested by Rempe and Dietrich (2014), though with some important differences. These results serve as a baseline for framing hypotheses that can inform more sophisticated analyses of field observations and numerical models.

ACKNOWLEDGMENTS

The authors would like to gratefully acknowledge the supported of National Science Foundation grants EAR-1344664, CBET-1360415 and EAR-90072546. Thanks to Susan Brantley and Daniella Rempe for the many stimulating discussions that motivated this work. Thanks also to two anonymous reviewers for helpful comments.

NOTATIONS

α	factor in thick weathering zone approximation that accounts for weathering front asymmetry
β	weathering model surface roughness factor
η	dimensionless ratio of parent rock mineral content and equilibrium concentration, adjusted for stoichiometry
∇h	total hydraulic head gradient
ω	rate of stream/valley incision (L T^{-1})
ϕ_m	final porosity once weathering is complete
ϕ, ϕ_0, ϕ_s	porosity, porosity of parent rock, porosity infilled by secondary precipitation
ρ	mineral density (M L^{-3})
θ	angle the (assumed impermeable) base of the aquifer B makes with the horizontal
A	mineral specific surface area (L^{-2} M^{-1})
C, C^{eq}, C^H	concentration, equilibrium concentration, and concentration of recharge (mol L^{-3})
D_m	molecular diffusion coefficient (L^{-2} T^{-1})
D	mineral grain diameter (L)

F_C, F_C^*	factor that accounts for the variations in K and C within the weathering front
F_W, F_W^*	factor that accounts for the variations in K within the weathering front
F	primary mineral molecular (formula) weight (M mol^{-1})
H_b	saturated thickness at the downslope boundary (L)
H_{bp}	thickness of the permeable unweathered bedrock at the downslope boundary (L)
H_D	diffusion length scales (L)
H_p, H_w, H_s	saturated thickness below the weathering zone, the thickness of weathering zone, and the saturated thickness above weathering zone (L)
H	total saturated thickness (L)
K	hydraulic conductivity (L T^{-1})
K_m	conductivity of rock once completely weathered (L T^{-1})
K_0	conductivity of unweathered rock (L T^{-1})
k, k^*	reaction rate [1/T], and area-specific reaction rate (mol L^{-2} T^{-1})
L	hillslope length (L)
M, M^0, M^H	mineral content, that of parent rock, and at $z = H$ (mol L^{-3})
n_{ij}, n	stoichiometric ratio of moles of solute product per mole of primary mineral
q_p	vertical flux from the weathering zone into the unweathered bedrock (L T^{-1})
q_w	vertical flux at the weathering front (L T^{-1})
q_x	horizontal component of Darcy flux (L T^{-1})
q_z^*	effective vertical flux adjusted for lateral variations in the saturated thickness (L T^{-1})
r	recharge rate (L T^{-1})
R	solute source term (mol L^{-3} T^{-1})
S	saturation index
w	weathering front advance rate (L T^{-1})
x	horizontal location along hillslope from divide, parallel to base B (L)
z_w	vertical co-ordinate where rock is half-weathered (L) ..
z'	vertical co-ordinate, moving frame of reference (L)
Z	scaled-vertical co-ordinate z/H
z	vertical co-ordinate, perpendicular to base B (L)

ORCID

Ciaran J. Harman https://orcid.org/0000-0002-3185-002X
Cassandra L. Cosans https://orcid.org/0000-0001-9121-532X

REFERENCES

Anderson, S. P., von Blanckenburg, F., & White, A. F. (2007). Physical and chemical controls on the critical zone. *Elements*, *3*(5), 315–319.

Bazilevskaya, E., Lebedeva, M., Pavich, M., Rother, G., Parkinson, D. Y., Cole, D., & Brantley, S. L. (2012). Where fast weathering creates thin regolith and slow weathering creates thick regolith. *Earth Surface Processes and Landforms*, *38*(8), 847–858.

Brantley, S. L., Holleran, M. E., Jin, L., & Bazilevskaya, E. (2013). Probing deep weathering in the Shale Hills Critical Zone Observatory, Pennsylvania (USA): The hypothesis of nested chemical reaction fronts in the subsurface. *Earth Surface Processes and Landforms*, *38*(11), 1280–1298.

Brantley, S. L., Lebedeva, M. I., Balashov, V. N., Singha, K., Sullivan, P. L., & Stinchcomb, G. (2017). Toward a conceptual model relating chemical reaction fronts to water flow paths in hills. *Geomorphology*.

Braun, J., Mercier, J., Guillocheau, F., & Robin, C. (2016). A simple model for regolith formation by chemical weathering. *Journal of Geophysical Research: Earth Surface*, *121*(11), 2140–2171.

Brutsaert, W. (2005). *Hydrology*. New York: Cambridge University Press.

Buss, H. L., Sak, P. B., Webb, S. M., & Brantley, S. L. (2008). Weathering of the Rio Blanco quartz diorite, Luquillo Mountains, Puerto Rico: Coupling oxidation, dissolution, and fracturing. *Geochimica Et Cosmochimica Acta*, *72*(18), 4488–4507.

Carmen, P. C. (1837). Flulid flow through granular beds. *Institution of Chemical Engineers*, *15*, 150–166.

Dixon, J. L., Heimsath, A. M., & Amundson, R. (2009). The critical role of climate and saprolite weathering in landscape evolution. *Earth Surface Processes and Landforms*, *34*(11), 1507–1521.

Harman, C. J., Cosans, C. L., & Putnam, S. M. (2017). Comment on "a simple model for regolith formation by chemical weathering" by Braun et al.: Contradictory concentrations and a tale of two velocities. *Journal of Geophysical Research-Earth Surface*, *122*(10), 2033–2036.

Harman, C. J., & Kim, M. (2018). A low-dimensional model of bedrock weathering and lateral flow coevolution in hillslopes: 1. Hydraulic theory of reactive transport, *Hydrological Processes* https://doi:10.1002/hyp.13360.

Harman, C. J., & Troch, P. A. (2014). What makes Darwinian hydrology "Darwinian"? Asking a different kind of question about landscapes. *Hydrology and Earth System Sciences*, *18*(2), 417–433.

Jones, E., Oliphant, T., & Peterson, P. (2001). SciPy: Open source scientific tools for Python. (*Tech. Rep.*) https://www.scipy.org/citing.html

Jung, H., & Navarre-sitchler, A. (2018a). Scale effect on the time dependence of mineral dissolution rates in physically heterogeneous porous media. *Geochimica Et Cosmochimica Acta*, *234*, 70–83.

Jung, H., & Navarre-sitchler, A. (2018b). Physical heterogeneity control on effective mineral dissolution rates. *Geochimica Et Cosmochimica Acta*, *227*, 246–263.

Kozeny, J. (1927). Ueber kapillare Leitung des Wassers im Boden. *Sitzungsberichte Wiener Akademie,136*, 271–306.

Lebedeva, M. I., & Brantley, S. L. (2013). Exploring geochemical controls on weathering and erosion of convex hillslopes: Beyond the empirical regolith production function. *Earth Surface Processes and Landforms*, *38*(15), 1793–1807.

Lebedeva, M. I., Fletcher, R. C., Balashov, V. N., & Brantley, S. L. (2007). A reactive diffusion model describing transformation of bedrock to saprolite. *Chemical Geology*, *244*(3-4), 624–645.

Lebedeva, M. I., Fletcher, R. C., & Brantley, S. L. (2010). A mathematical model for steady-state regolith production at constant erosion rate. *Earth Surface Processes and Landforms*, *35*(5), 508–524.

Li, D. D., Jacobson, A. D., & McInerney, D. J. (2014). A reactive-transport model for examining tectonic and climatic controls on chemical weathering and atmospheric CO2 consumption in granitic regolith. *Chemical Geology*, *365*, 30–42.

Li, L., Maher, K., Navarre-sitchler, A., Druhan, J., Meile, C., Lawrence, C., ... Beisman, J. (2017). Expanding the role of reactive transport models in critical zone processes. *Earth-Science Reviews*, *165*, 280–301.

Lichtner, P. C. (1988). The quasi-stationary state approximation to coupled mass transport and fluid-rock interaction in a porous medium. *Geochimica Et Cosmochimica Acta*, *52*(1), 143–165.

Maher, K. (2011). The role of fluid residence time and topographic scales in determining chemical fluxes from landscapes. *Earth and Planetary Science Letters*, *312*(1-2), 48–58.

Manning, A. H., Verplanck, P. L., Caine, J. S., & Todd, A. S. (2013). Links between climate change, water-table depth, and water chemistry in a mineralized mountain watershed. *Applied Geochemistry*, *37*, 64–78.

Murphy, W. M., Oelkers, E. H., & Lichtner, P. C. (1989). Surface reaction versus diffusion control of mineral dissolution and growth rates in geochemical processes. *Chemical Geology*, *78*(3-4), 357–380.

Navarre-sitchler, A., Steefel, C. I., Yang, L., Tomutsa, L., & Brantley, S. L. (2009). Evolution of porosity and diffusivity associated with chemical weathering of a basalt clast. *Journal of Geophysical Research*, *114*(F2), 1–14.

Nettleton, W. D., Flach, K. W., & Nelson, R. E. (1970). Pedogenic weathering of tonalite in southern California. *Geoderma*, *4*(4), 387–402.

Ortoleva, P., Merino, E., Moore, C., & Chadam, J. (1987). Geochemical self-organization, I; reaction-transport feedbacks and modeling approach. *American Journal of Science*,*287*, 979–1007. https://doi:10.2475/ajs.287.10.979

Parizek, J. R., & Girty, G. H. (2014). Catena assessing volumetric strains and mass balance relationships resulting from biotite-controlled weathering: Implications for the isovolumetric weathering of the Boulder Creek Granodiorite, Boulder County,. *Catena*, *120*, 29–45.

Phillips, J. D. (2005). Deterministic chaos and historical geomorphology: A review and look forward. *Geomorphology*, *76*, 109–121.

Portenga, E. W., & Bierman, P. R. (2011). Understanding Earth's eroding surface with 10Be. *Gsa Today*, *21*(8), 4–10.

Rempe, D. M., & Dietrich, W. E. (2014). A bottom-up control on fresh-bedrock topography under landscapes. *Proceedings of the National Academy of Sciences*, *111*(18), 6576–6581.

Riebe, C. S., Hahm, W. J., & Brantley, S. L. (2017). Controls on deep critical zone architecture: A historical review and four testable hypotheses. *Earth Surface Processes and Landforms*, *42*(1), 128–156.

Riebe, C. S., Kirchner, J. W., & Finkel, R. C. (2004). Erosional and climatic effects on long-term chemical weathering rates in granitic landscapes spanning diverse climate regimes. *Earth and Planetary Science Letters*, *224*(3-4), 547–562.

Roberts, S. M., & Shipman, J. S. (1972). *Two-point boundary value problems: Shooting methods*, Modern analytic and computational methods in science and mathematics, No. 31: American Elsevier Pub. Co. New York.

St Clair, J., Moon, S., Holbrook, W. S., Perron, J. T., Riebe, C. S., Martel, S. J., ... Richter, D. D. (2015). Geophysical imaging reveals topographic stress control of bedrock weathering. *Science (New York, N.Y.)*, *350*(6260), 534–538.

Toth, J. (1963). A theoretical analysis of groundwater flow in small drainage basins. *Journal of Geophysical Research*, *68*(16), 4795–4812.

White, A. F., & Blum, A. E. (1995). Effects of climate on chemical weathering in watersheds. *Geochimica Et Cosmochimica Acta*, *59*(9), 1729–1747.

White, A. F., & Brantley, S. L. (2003). The effect of time on the weathering of silicate minerals: Why do weathering rates differ in the laboratory and field? *Chemical Geology*, *202*(3-4), 479–506.

Xu, P., & Yu, B. (2008). Developing a new form of permeability and Kozeny – Carman constant for homogeneous porous media by means of fractal geometry. *Advances in Water Resources*, *31*, 74–81.

How to cite this article: Harman CJ, Cosans CL. A low-dimensional model of bedrock weathering and lateral flow co-evolution in hillslopes: 2. Controls on weathering and permeability profiles, drainage hydraulics, and solute export pathways. *Hydrological Processes*. 2019;1–23. https://doi.org/10.1002/hyp.13385

APPENDIX A: SOLUTION METHOD FOR THICK WEATHERING FRONT APPROXIMATION

The integrals in (30), (31), and (34) can be solved by approximating the variations in $C(z)$ and $M(z)$ as straight lines. We can assume that $C \approx C^{eq}$ and $M = M^0$ at the bottom of the weathering zone $z = H_p$ and the upper boundary condition give $C \approx C^H$ at the top of the weathering zone $z = H_p + H_w$. Numerical results and the analytical solutions suggest that M will vary with a slope given by $M^0/(2\delta)$ (which is the rate of change at the inflection point z_w). Thus, we can approximate

$$M(z) \approx M^0 \left(1 - \frac{z - H_p}{2\delta}\right) \tag{A1}$$

$$C(z) \approx C^H + (C^{eq} - C^H)\left(1 - \frac{z - H_p}{2\delta f}\right), \tag{A2}$$

where $f = H_W/(2\delta)$.

We also simplify the Kozeny–Carmen relation (10) by assuming that most variation in K is due to variation in the numerator ϕ^3 rather than the denominator $(1 - \phi)^2$, so $K = K_0(\phi/\phi_0)^3$. The maximum permeability is therefore $K_m = K_0((\phi_0 + \phi_m)/\phi_0)^3$. This will be true so long as ϕ is small. By substituting the linear approximation for M (A1) into (9) and then (10), we can obtain

$$\begin{aligned} F_W(k) &= \int_{H_p}^{H_p + k2\delta} \frac{K(z)}{2\delta K_m} dz \\ &= \int_0^k (\zeta + \Phi - \zeta\Phi)^3 d\zeta \\ &= \frac{\Omega_k^4 - \Phi^4}{4(1 - \Phi)}, \end{aligned} \tag{A3}$$

where $\Phi = \phi_0/\phi_m$ and $\Omega_k = k + \Phi - k\Phi$. This allows us to write (30) as

$$rx = -q_p x + H_w F_W(f) K_m |\Delta h| + H_s K_m |\Delta h|, \tag{A4}$$

where $-q_p x = H_p K_0 |\nabla h|$ is the water flux below the weathering zone and F_W is evaluated at $k \to f = H_W/(2\delta)$. We can also write (34) as

$$-q_w x = -q_p x + 2\delta F_W(\alpha) K_m |\Delta h|, \tag{A5}$$

where

$$\alpha = (z_w - H_p)/(2\delta) \tag{A6}$$

gives the relative location of z_w within H_w. In completely submerged profiles, we would expect this to be close to $\alpha = 0.5$.

For (31), we have to account for the fact that the concentration is also varying in z. Using the same linear approximations, we can write

$$\begin{aligned} F_C(f) &= \int_{H_p}^{H_p + f2\delta} \frac{C(z)K(z)}{C^{eq} 2\delta K_m} dz \\ &= \int_0^f \left(1 - \left(1 - \frac{C^H}{C^{eq}}\right)\frac{\zeta}{f}\right)(\zeta + \Phi - \zeta\Phi)^3 d\zeta \\ &= \frac{5\left(\Omega_f^4 - \Phi^4\right)\left(\Omega_f - \Phi\frac{C^H}{C^{eq}}\right) - 4\left(1 - \frac{C^H}{C^{eq}}\right)\left(\Omega_f^5 - \Phi^5\right)}{20f(1 - \Phi)^2}, \end{aligned} \tag{A7}$$

where $\Omega_f = f + \Phi - f\Phi$. This allows us to write (35).

F_W^* and F_C^* refer to the values of $F_W(f)$ and $F_C(f)$ when $f = 1$. Parameters for base case example give $F_W^* = 0.54$ and $F_C^* = 0.2$. In completely submerged profiles, α is typically slightly larger than 0.5 but is smaller in incompletely submerged profiles.

To find values of z_w and δ using this approximation, we used the following procedure:

1. Calculate initial estimates $q_p = q_w = \eta\omega$ and $\delta = 2\omega/k$.
2. f is determined by checking whether $(r - q_p)x > 2\delta F_W^* K_0 |\nabla h|$. If it is, we set $f = 1$, and (A4) can be used to find H_s. If not, $H_s = 0$ and Equations A4 and A3 can be inverted to obtain f.
3. The value of f is used to determine F_C from (A7) and a new estimate of q_p from (35).
4. Steps 2 and 3 are iterated to find a consistent value of q_p.
5. Equations A5 and A3 can be inverted to obtain α.
6. The values of α and f can then be fed into (A6) and (29) to obtain estimates of z_w and H.
7. Equation 32 is used to obtain a new estimate of q_w.
8. Steps 5–7 are iterated to find a consistent value of q_w.
9. Equation 27 is used to obtain a new estimate of δ
10. Steps 2–9 are iterated to obtain a consistent value of δ.

APPENDIX B: DETERMINATION AND EVALUATION OF CONSTANTS IN THE DIFFUSION SOLUTION

The solution to (1) under the given conditions can be expressed succinctly as

$$C(x,z) = C^{eq} + cH_D(x)\sqrt{\frac{\pi}{4}}\,\mathrm{Erf}\left(\frac{z}{H_D(x)}\right), \tag{B1}$$

where c is a constant of integration. To determine c, we can apply the condition that the rate of diffusion away from the lower boundary upslope of x is equal to the rate of removal by lateral flow at x. The rate of transport into the aquifer by diffusion is given by

$$\text{Mass in} = \int_0^x -\phi D_m \left.\frac{\partial C}{\partial z}\right|_{z=0} dx, \tag{B2}$$

$$= -c\phi D_m x. \tag{B3}$$

The rate of removal is obtained by integrating the product of the lateral flow and the vertical profile of concentration $q_x C$ from $z = 0$ to $z = H$:

$$\text{Mass in} = \int_0^H q_x C\, dz, \tag{B4}$$

$$= C^{eq} H q_x - c\phi D_m x\left(1 - \exp\left(-\frac{H^2}{H_D^2}\right) - \sqrt{\pi}\frac{H}{H_D}\mathrm{Erf}\left(\frac{H}{H_D}\right)\right). \tag{B5}$$

Equating these and solving for c yields

$$c = -\frac{2C^{eq}\gamma}{H_D\sqrt{\pi}}, \tag{B6}$$

where γ is given by

$$\gamma = \left(\exp\left(-\frac{H^2}{H_D^2}\right) / \left(\sqrt{\pi}\frac{H}{H_D}\right) + \mathrm{Erf}\left(\frac{H}{H_D}\right)\right)^{-1}. \tag{B7}$$

The value of γ is very nearly 1 for $H > H_D$ (indeed for $H = H_D$ $\gamma = 0.95$, and for $H = 2H_D$ $\gamma = 0.9995$). Given the base case parameters, the value of H at which $H = H_D$ is 0.0315 m. For all H greater than this, the steady-state concentration distribution will be well approximated by

$$C(x,z) = C^{eq}\ \mathrm{Erfc}\left(\frac{z}{H_D}\right). \tag{B8}$$